X-612-68-328

PREPRINT

NASA TM X- 63320

TEMPORAL VARIATIONS OF THE 100 keV TO 1700 keV TRAPPED PROTONS OBSERVED ON SATELLITE EXPLORER 26 DURING FIRST HALF OF 1965

F. SORAAS

L. R. DAVIS

AUGUST 1968

GSFC

GODDARD SPACE FLIGHT CENTER

GREENBELT, MARYLAND

X-612-68-328

TEMPORAL VARIATIONS OF THE 100 keV TO 1700 keV TRAPPED PROTONS OBSERVED ON SATELLITE EXPLORER 26 DURING FIRST HALF OF 1965

F. Söraas*
L. R. Davis

August 1968

*NASA-NAS Postdoctoral Resident Research Associate

GODDARD SPACE FLIGHT CENTER
Greenbelt, Maryland

TEMPORAL VARIATIONS OF THE 100 keV TO 1700 keV TRAPPED PROTONS OBSERVED ON SATELLITE EXPLORER 26 DURING FIRST HALF OF 1965

F. Söraas*
L. R. Davis

ABSTRACT

The temporal behavior of 100 keV geomagnetically-trapped protons in the region 2 to 5.5 earth radii for the period 29 January through 29 June 1965 has been determined using data from a scintillation detector on Explorer 26. The results exhibit both adiabatic changes which vary directly with the magnetic field (Dst) and non-adiabatic changes which do not track the field. The adiabatic variations, which result from slow changes in fields during which all three adiabatic invariants are conserved, can be removed by transforming the measurements from the time dependent field to a reference field. We have computed the transformation for protons mirroring on the equator using a disturbance field, $B(t, L) = C \cdot Dst(t) \cdot f(L)$ where C is a constant (~ 0.7) that corrects for the induction field of the conducting earth, t is the time of observation and $f(L)$ is the radial dependence for a model ring current field. The transformation reduce the regression coefficients of proton intensity on Dst by a factor of 5 or more out to $L = 4.5$. The transformed data clearly show non-adiabatic variations. The protons underwent rapid changes during magnetic storms. Those having energies less than about 200 keV were enhanced by as much as a factor of four while the higher energy protons were depleted by as much as a factor of ten. Following the storm-time-changes both lower and higher energy protons slowly recovered toward their prestorm values. The recovery rates increase with increasing L-value. The particle data for periods when the non-adiabatic changes were small have been used to determine values for C which agree with values derived from surface measurements of field fluctuations.

*NASA-NAS Postdoctoral Resident Research Associate.

CONTENTS

TEMPORAL VARIATIONS OF THE 100 keV TO 1700 keV TRAPPED PROTONS OBSERVED ON SATELLITE EXPLORER 26 DURING FIRST HALF OF 1965

INTRODUCTION

The low energy protons in the outer radiation belt were first studied extensively by Davis and Williamson (1963) with an instrument flown on Explorer 12 in 1961. They found fluxes of protons with energies greater than 100 keV as large as 6×10^7 per cm^2-sec-sr with a maxima at L = 3.5 earth radii. Later they obtained additional measurements on Explorer 14 and 15 in 1962, when solar activity was still high, and on Explorer 26 in 1965, which is near solar minimum. The results of these and other measurements, Davis et al. (1964), Davis (1965), Mihalov et al. (1966), Armstrong et al. (1968), and Burns (1968), have shown that protons of these energies; (1) are trapped throughout the region from L = 2 to the outer boundary of the trapping region, (2) have spectra which soften with increasing radial distance, (3) remain relatively stable out to five earth radii during magnetically quiet times, and (4) undergo changes down to L = 3 during larger magnetic disturbances and in the region above L = 5 even during small magnetic disturbances.

In a theoretical study Nakada et al. (1965a) have shown that the distribution of these protons is as predicted from radial transport conserving the first two invariants of particle motion. These results, along with those of Nakada et al. (1965b), suggest that radial diffusion plays an important part in populating the radiation belt and that the source of the outer belt protons is near the magnetopause, rather than near the earth. Kennel and Petschek (1966) proposed another non-adiabatic process, pitch angle scattering by VLF radio waves, which they show sets an upper limit on the intensity of protons that can be stably trapped.

Dessler et al. (1961), McIlwain (1966a), and others have shown that the adiabatic changes in the trapped particles, which result from particles responding to slow changes in the geomagnetic field while conserving all three invariants, product significant changes in the observed intensities. Thus, continuous observations must be corrected for adiabatic effects before they can be used for detailed studies of the non-adiabatic processes.

In order to study the possible source, loss, and transport mechanisms responsible for the proton behavior we need a set of continuous observations spanning a time period long compared to the time scale of the processes operating on the protons. In an attempt to satisfy this requirement we have analyzed Explorer 26 proton data for the period 29 January to 29 June 1965. The present

paper presents the results and describes a method which has been used to correct the data for the adiabatic effects.

INSTRUMENTATION

The scintillation detector flown on Explorer 26 measured the directional intensity of 100 keV to about 10 MeV protons in a pulse counting mode and the directional energy flux of 10 keV to 100 keV electrons in a current mode. Details of the detector have been given by Davis and Williamson (1963) and Davis (1965). In the pulse mode the detector counted low energy ions losing more than 80 keV energy in 2.5 mg/cm^2 thick ZnS(Ag:Cl) powder phospher. Proton energy spectra were obtained by interposing, in time sequence, eight nickel foils in front of the detector. Figure 1 shows the proton count rate efficiencies as a function of proton energy for the eight foils. The count rate of the detector

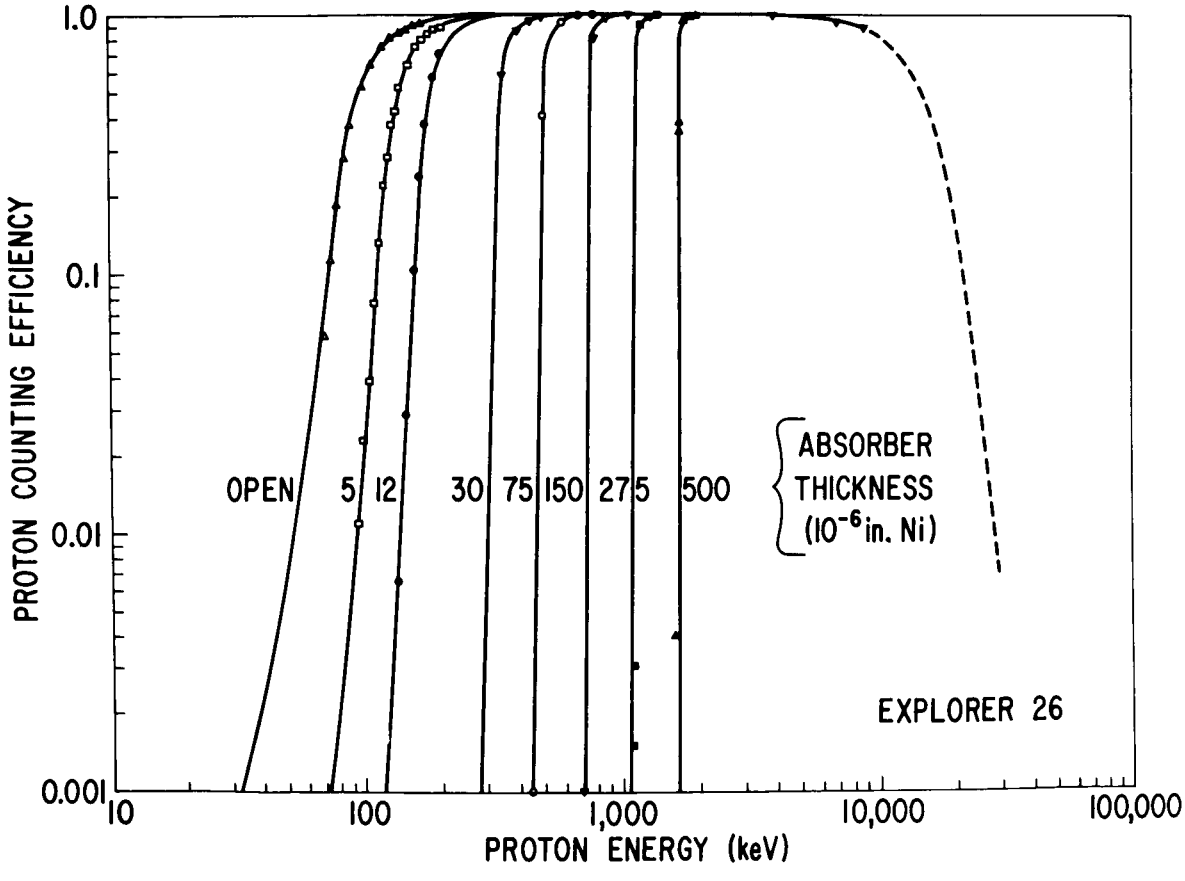

Figure 1. Detector count rate efficiency curves.

is given by

$$R = G\int_0^{\alpha} \epsilon(E)\, j(E)\, dE \tag{1}$$

where G is the telescope factor in cm^2-sr, $\epsilon(E)$ is the count rate efficiency, and $j(E)$ is the differential directional intensity of the protons. We have converted the observed count rates to integral proton intensities using

$$J(>E^*) = \frac{R}{G} \tag{2}$$

where E^* is defined by

$$\int_{E^*}^{\alpha} j(E)\, dE = \int_0^{\alpha} \epsilon(E)\, j(E)\, dE \tag{3}$$

We have evaluated E^* for exponential spectra having e-folding energies from 100 keV to 2000 keV and found that the values are constant to within ±15 keV. Table 1 lists the eight absorber thicknesses, preliminary E^* values used in this analysis, and the telescope factors, and the telescope full-cone angle. Since completion of the present study additional preflight calibration data have been reduced which give E^* values 6 keV to 20 keV larger. However, the errors thus introduced in the present analysis should not greatly affect the results presented here.

The Explorer 26 satellite was launched on December 21, 1964, into an orbit having inclination of 20.1°, an orbital period of ~7.5 hours, an apogee of 26,000 km altitude and perigee of 200 km. Thus the radial dependence over the range 1-5 earth radii of the particle fluxes near the equatorial plane can be obtained up to six times each day. During the time period considered here, January 29, 1965, through June 29, 1965, the apogee of the orbit precessed through the local time interval of 1618 hours to 1121 hours. The satellite spin rate gradually and uniformly slowed from about 28 rpm to 9 rpm during this period.

Table 1

Nickel Absorber Thickness, Effective Low-Energy Cutoffs, Telescope Factors, and Telescope Full Viewing Angles of Explorer 26 Detector.

Ni Absorber Thickness (10^{-6} inches)	Effective Cut-Off Energies (keV)	Telescope Factors (cm^2-sr)	Full Opening Angle (degrees)
zero	98	3.46×10^{-5}	11.4°
5	134	3.46×10^{-5} 6.84×10^{-3}	11.4°* 20.6°
12	180	3.46×10^{-5}	11.4°
30	345	3.46×10^{-5} 6.84×10^{-3}	11.4°* 20.6°
75	513	2.63×10^{-4}	12.6°
150	775	2.63×10^{-4}	12.6°
275	1140	9.64×10^{-4}	14.2°
500	1700	3.20×10^{-3}	17.6°

*To increase the dynamic range there were two each of the 5 and 30 millionths inch thick absorbers with large and small aperatures.

The detector axis was oriented at 45° to the satellite spin-axis and particle counts were accumulated and telemetered every 0.29 seconds, a small fraction of a roll period, to permit measuring intensity as a function of pitch-angle. We have chosen to order our data in an L-equatorial pitch angle (EPA) coordinate system. Our detector, with the aid of an optical aspect sensor on the satellite, measured the directional intensity of particles in inertial coordinates. We then determined the local pitch angle (LPA) of the particles being measured, using a computed value of the field direction. Assuming the conservation of the magnetic moment invariant the EPA was determined from

$$\sin^2 \text{EPA} = \frac{B_0}{B} \sin^2 \text{LPA} \tag{4}$$

where B is the field intensity at the satellite and B_0 the minimum intensity on the field line. It should be noted that the L-values have been computed for the spacecraft location and not for the mirroring point of the particles being sampled. That is ignoring L-shell splitting. However, the errors thus introduced are small and probably less than the errors that result from using Jensen and Cain (1962) magnetic field model, which does not include terms from external currents.

The stability of the detector was checked in flight by means of a radioactive alpha source. The results show that the analog count rate circuit was stable to within about 10% throughout the period under investigation. The low energy cut-offs were determined by the energy loss in the absorbers plus an 80 keV electronic threshold. While the alpha source calibration indicates that the threshold was stable it was not a very sensitive measure of the threshold. The consistency of the measured proton fluxes at low L values is a good indication that the electronic threshold was stable throughout the period.

ANALYSIS OF THE DATA

In order to study the temporal behavior of the integral proton intensities at different energies, L-values, and pitch angles, a regression function

$$\log J(>E) = A_1 + A_2 \cdot \cos^2 EPA + A_3 \cdot (L - L_0) + A_4 \cdot \cos^2 EPA \cdot (L - L_0) \quad (5)$$

is fitted to each of the eight integral intensities by means of a least square calculation. This calculation is performed for every half L-value from L = 2 to L = 5.5. For each fit data, in the interval $L_0 \pm 0.1$ earth radii and EPA greater than 42.5° are used. Logarithm to the base 10 is used, L_0 is the central L-value and J(> E) is the proton integral intensity. A_1 gives the log of the intensities of particles mirroring at the equator, i.e. EPA = 90°. A_2 tells how the log intensity depends on the pitch angle. A_3 gives the L dependence of the log intensity, and A_4 takes care of the fact that the pitch angle distribution is L-dependent.

We have found that the pitch angle dependence for EPA greater than approximately 42.5° is very well represented by a straight line when log J (> E) is plotted versus $\cos^2$ EPA (i.e. over the range $0.0 \leq \cos^2 EPA \leq 0.54$). At smaller pitch angles the measured intensity falls below the straight line. This pitch angle dependence can be seen in Figure 2 which shows the measured proton intensities plotted against $\cos^2$ EPA. The right hand side of the figure shows the

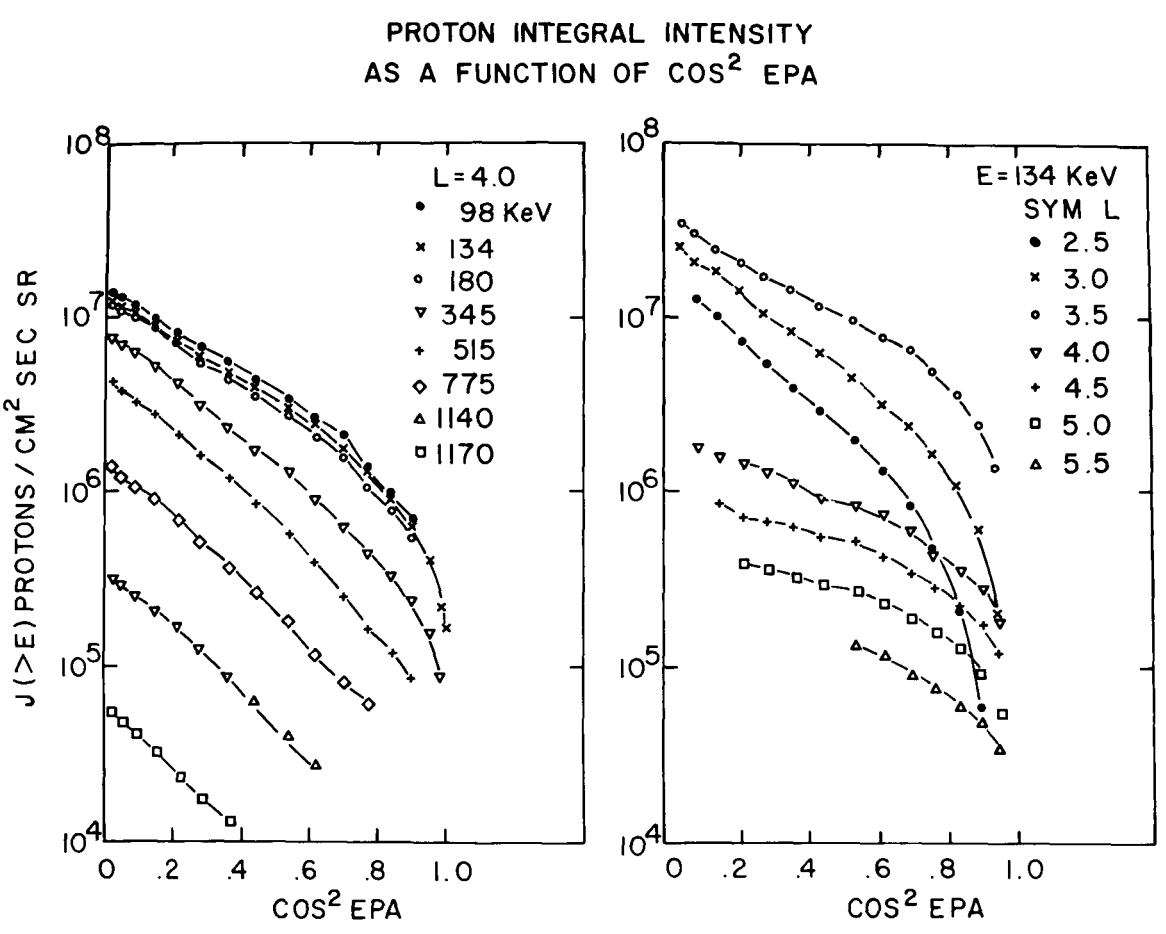

Figure 2. Measured proton intensities plotted vs. $\cos^2$ EPA. The right-hand side of the figure shows the pitch angle dependence for protons greater than 134 keV at a number of different L-values. The left-hand side of the same figure shows the pitch angle dependence for all eight integral energies at L = 4. Notice that the curves are almost straight lines for $\cos^2$ EPA less than 0.54, i.e. EPA $\geq 42.5°$.

pitch angle dependence for protons greater than 134 keV at a number of L-values and the left hand side shows the pitch angle dependence for all eight integral energies at L = 4.0.

The regression function (5) represents the data rather well. The standard deviation, the RMS around the fitted surface, together with the standard deviation of the regression coefficients A_1 to A_4 and the correlation index I were computed. I is defined in the same way as the correlation coefficient and is given by

$$I = \left(1 - RMS^2/S^2\right)^{1/2} \qquad (6)$$

where S^2 is the variance in log of J (>E). Typical values of the uncertainties associated with the determination of A_1 and A_2 for different L-values and energies are given in Table 2 together with values of the correlation index. These values, obtained for the days January 29 through February 4, are representative for the whole period under investigation.

Table 2

Typical values of the standard deviation of A1 and A2 together with the standard deviation (RMS) around the log J Surface. For all three the units are log 10 (protons/cm^{2}s.sr). The Correlation coefficient I is also given.

L-Value	δA1	δA2	RMS	I	Energy (keV)
2.5	0.03	0.07	0.07	0.86	98
3.0	0.02	0.03	0.06	0.86	"
3.5	0.02	0.03	0.06	0.80	"
4.0	0.03	0.04	0.07	0.74	"
4.5	0.02	0.03	0.07	0.70	"
5.0	0.02	0.02	0.09	0.65	"
5.5	0.05	0.11	0.15	0.37	"
2.5	0.03	0.06	0.07	0.89	180
3.0	0.02	0.03	0.05	0.88	"
3.5	0.02	0.03	0.05	0.83	"
4.0	0.03	0.03	0.06	0.79	"
4.5	0.02	0.03	0.08	0.74	"
5.0	0.02	0.04	0.13	0.61	"
5.5	0.04	0.12	0.16	0.25	"
2.5	0.02	0.03	0.04	0.97	1140
3.0	0.02	0.02	0.03	0.94	"
3.5	0.02	0.02	0.04	0.92	"
4.0	0.05	0.05	0.09	0.85	"
4.5	0.03	0.09	0.16	0.50	"
5.0	0.02	0.10	0.08	0.35	"

The integral proton intensity at $L = L_0$ as a function of EPA is given by

$$\log J(>E) = A_1 + A_2 \cdot \cos^2 EPA \qquad (7)$$

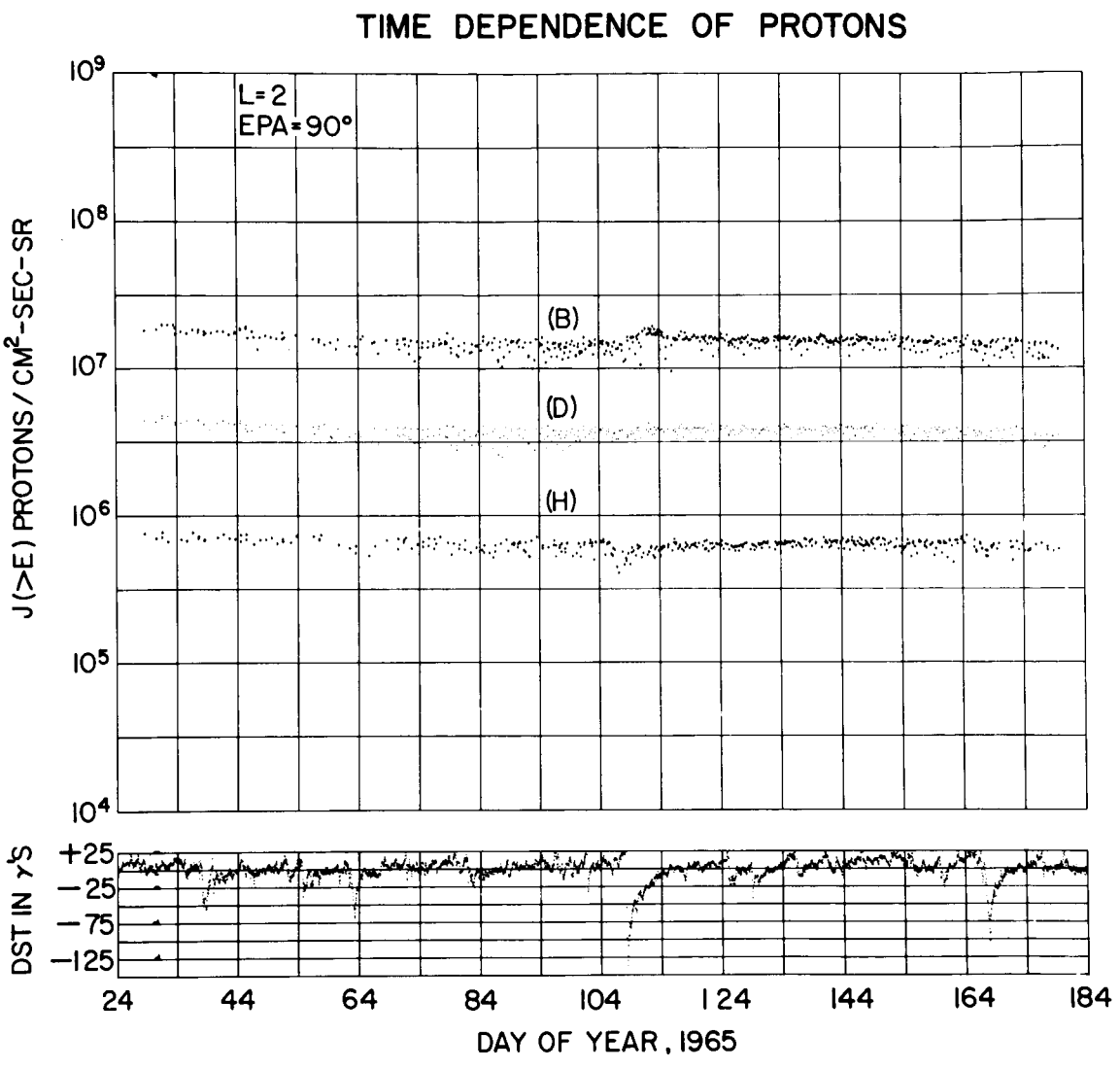

Figure 3. The time behavior of protons mirroring at the equator for three integral energies measured at L = 2. The different curves are marked with letters B, D and H corresponding to the energies 134, 345, and 1700 keV. The curves are displaced in order to avoid overlap and the values read from the curves B, D and H must be multiplied by 10 raised to the following exponents -0.75, -0.25, and 0.25 in order to get the integral proton intensity above a certain energy in protons/cm^2 sec sr. Below the proton data are plotted the hourly average Dst values.

RESULTS

Figures 3 through 10 show the time behavior of protons mirroring at the equator for the eight integral energies measured by the scintillator in the L-range 2 to 5.5. They are plots of A_1 in Equation (7) vs. time. On the same

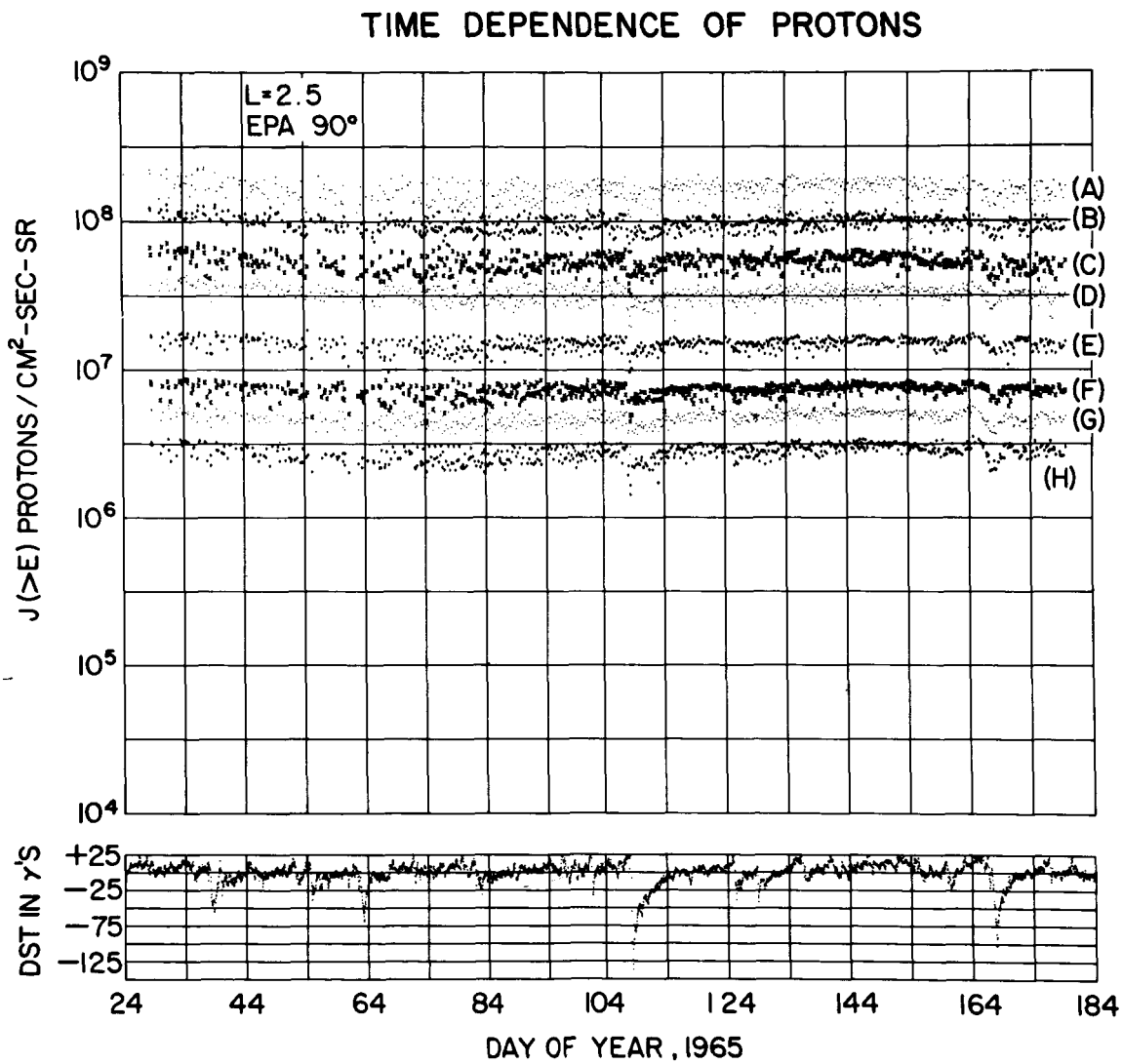

Figure 4. The time behavior of protons mirroring at the equator for the eight integral energies measured at L = 2.5. The different curves are marked with letters running from A to H corresponding to the energies 98, 134, 180, 345, 513, 775, 1140 and 1700 keV. The curves are displaced in order to avoid overlap and the values read from the curves A to H must be multiplied by 10 raised to the following exponents -1, -0.75, -0.50, -0.25, 0.0, 0.25, 0.25 and 0.25 in order to get the integral proton intensity above a certain energy in protons/cm^2 sec sr. Below the proton data are plotted the hourly average Dst values.

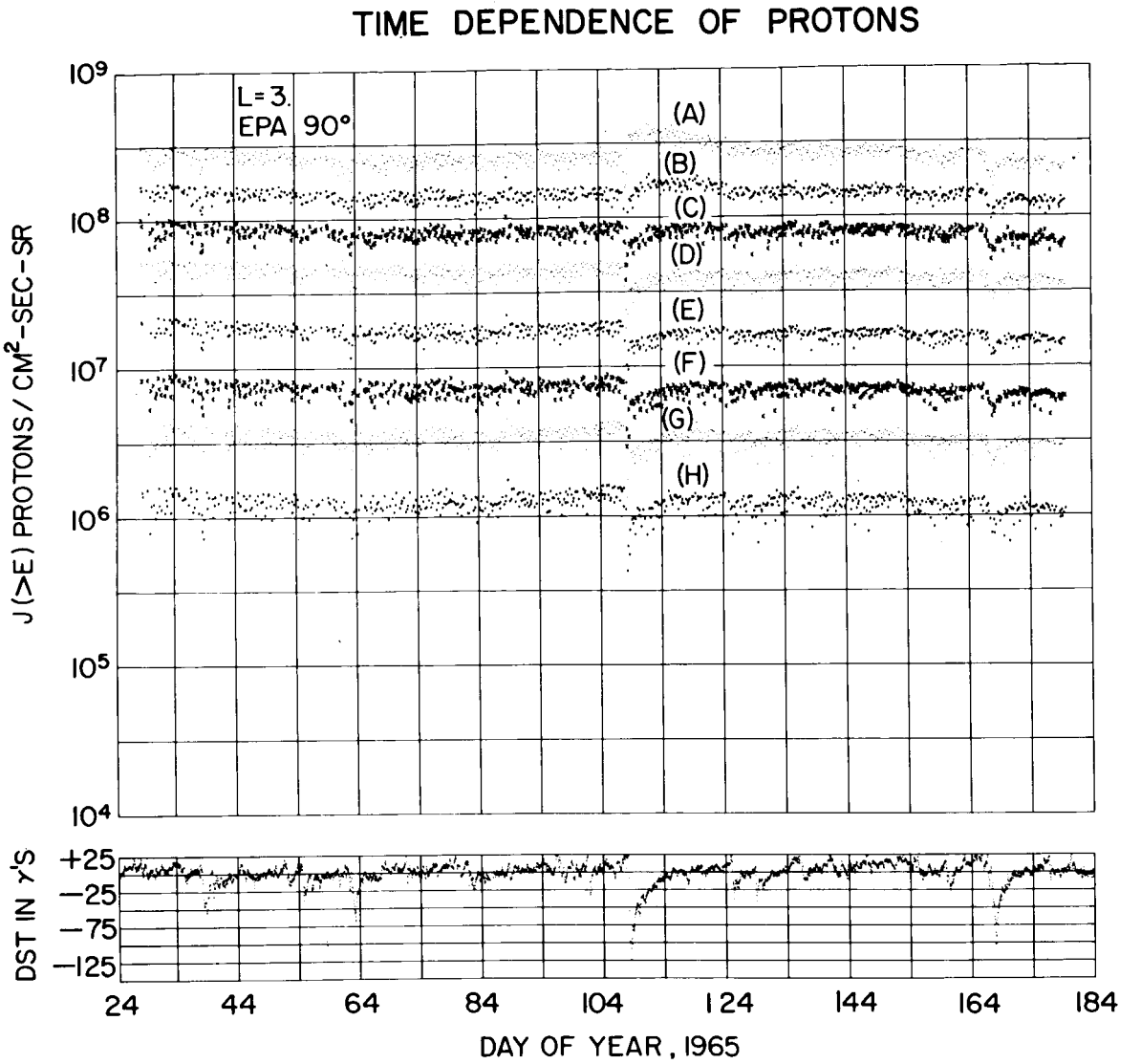

Figure 5. The time behavior of protons mirroring at the equator for the eight integral energies measured at L = 3. The different curves are marked with letters running from A to H corresponding to the energies 98, 134, 180, 345, 513, 775, 1140 and 1700 keV. The curves are displaced in order to avoid overlap and the values read from the curves A to H must be multiplied by 10 raised to the following exponents -1, -0.75, -0.50, -0.25, 0.0, 0.25, 0.25 and 0.25 in order to get the integral proton intensity above a certain energy in protons/cm^2 sec sr. Below the proton data are plotted the hourly average Dst values.

plots the magnetic variations as given by Dst is shown. Dst values are computed by Sugiura and Hendricks of Goddard Space Flight Center and is a measure of the variation of the magnetic field near the earths equator, averaged in longitude.

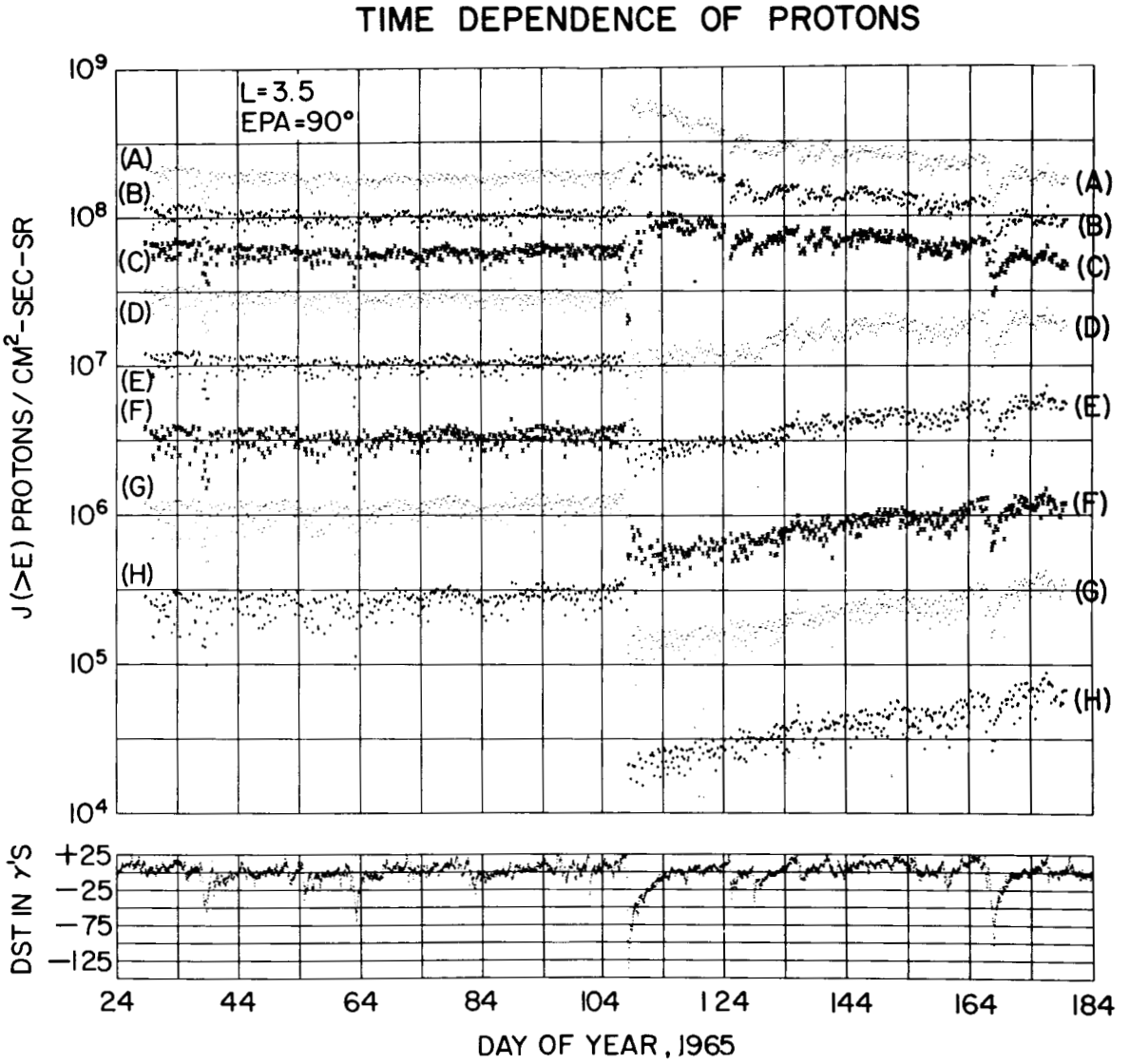

Figure 6. The time behavior of protons mirroring at the equator for the eight integral energies measured at L = 3.5. The different curves are marked with letters running from A to H corresponding to the energies 98, 134, 180, 345, 513, 775, 1140 and 1700 keV. The curves are displaced in order to avoid overlap and the values read from the curves A to H must be multiplied by 10 raised to the following exponents -1, -0.75, -0.50, -0.25, 0.0, 0.25, 0.25 and 0.25 in order to get the integral proton intensity above a certain energy in protons/cm^2 sec sr. Below the proton data are plotted the hourly average Dst values.

The most obvious features of these plots are:

1. At all L-values there are variations in the proton fluxes which exhibit a close correlation with variations in Dst. This can be seen explicitly by making a regression analysis of log J(> E) with respect to Dst and time

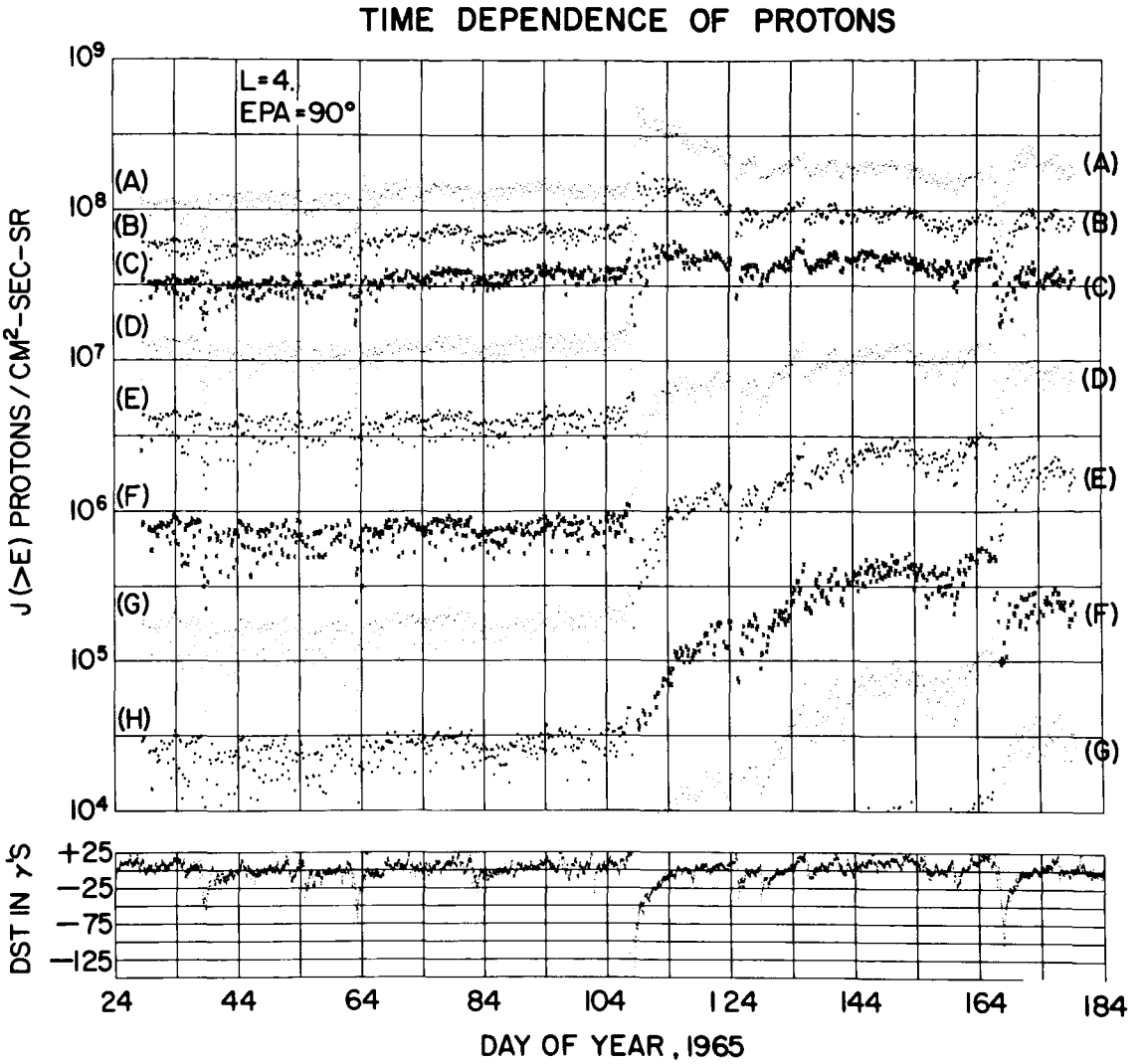

Figure 7. The time behavior of protons mirroring at the equator for the eight integral energies measured at L = 4. The different curves are marked with letters running from A to H corresponding to the energies 98, 134, 180, 345, 513, 775, 1140 and 1700 keV. The curves are displaced in order to avoid overlap and the values read from the curves A to H must be multiplied by 10 raised to the following exponents -1, -0.75, -0.50, -0.25, 0.0, 0.25, 0.25 and 0.25 in order to get the integral proton intensity above a certain energy in protons/cm^2 sec sr. Below the proton data are plotted the hourly average Dst values.

(t) during a selected time-period using the function

$$\log J(>E) = B_1 + B_2 \cdot Dst + B_3 \cdot t + B_4 \cdot t^2 \qquad (8)$$

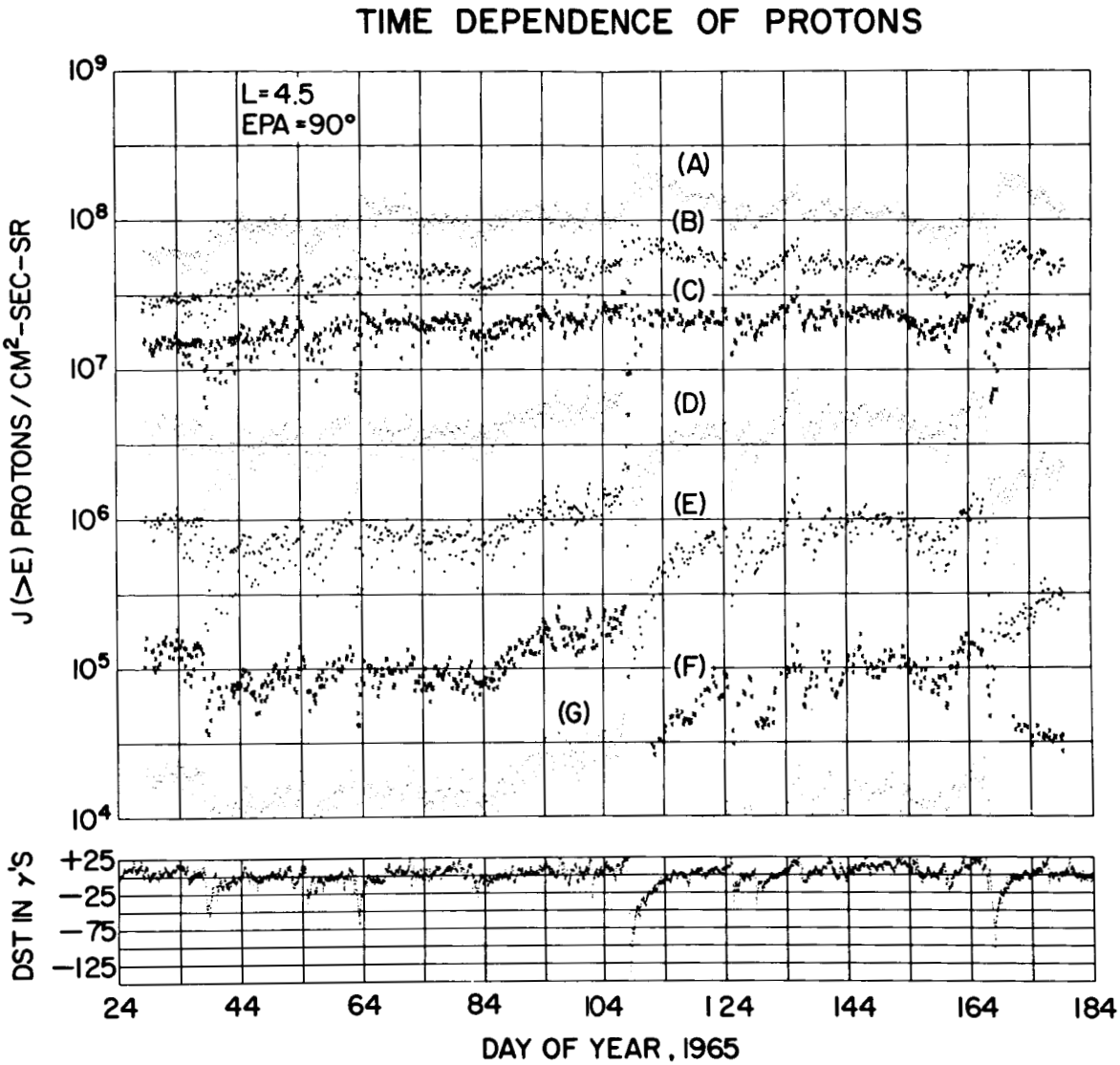

Figure 8. The time behavior of protons mirroring at the equator for seven integral energies measured at L = 4.5. The different curves are marked with letters running from A to G corresponding to the energies 98, 134, 180, 345, 513, 775, and 1140 keV. The curves are displaced in order to avoid overlap and the values read from the curves A to G must be multiplied by 10 raised to the following exponents -1, -0.75, -0.50, -0.25, 0.0, 0.25, and 0.25 in order to get the integral proton intensity above a certain energy in protons/cm^2 sec sr. Below the proton data are plotted the hourly average Dst values.

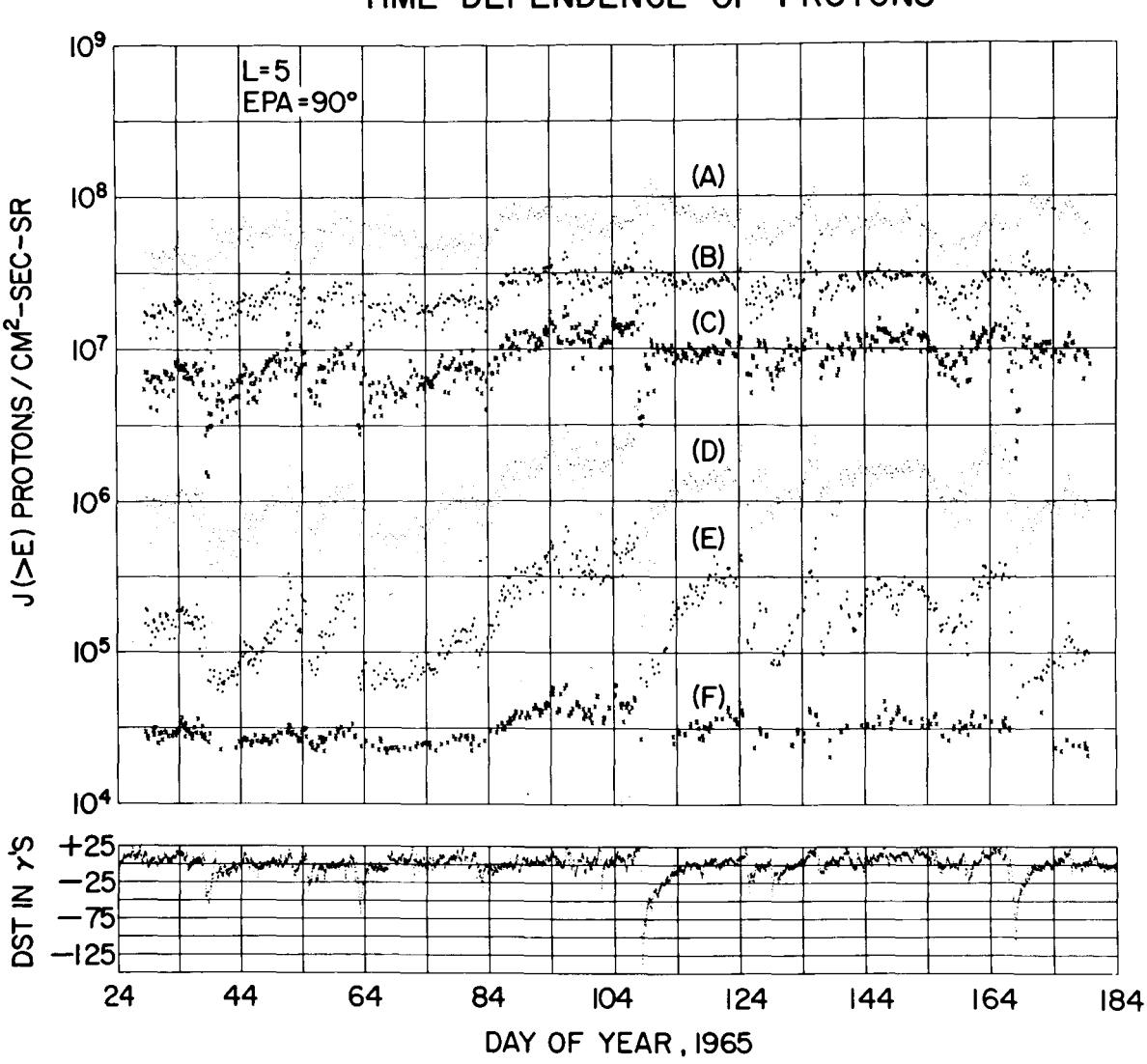

Figure 9. The time behavior of protons mirroring at the equator for six integral energies measured at L = 5. The different curves are marked with letters running from A to F corresponding to the energies 98, 134, 180, 345, 513, and 775 keV. The curves are displaced in order to avoid overlap and the values read from the curves A to F must be multiplied by 10 raised to the following exponents -1, -0.75, -0.50, -0.25, 0.0, and 0.25 in order to get the integral proton intensity above a certain energy in protons/cm^2 sec sr. Below the proton data are plotted the hourly average Dst values.

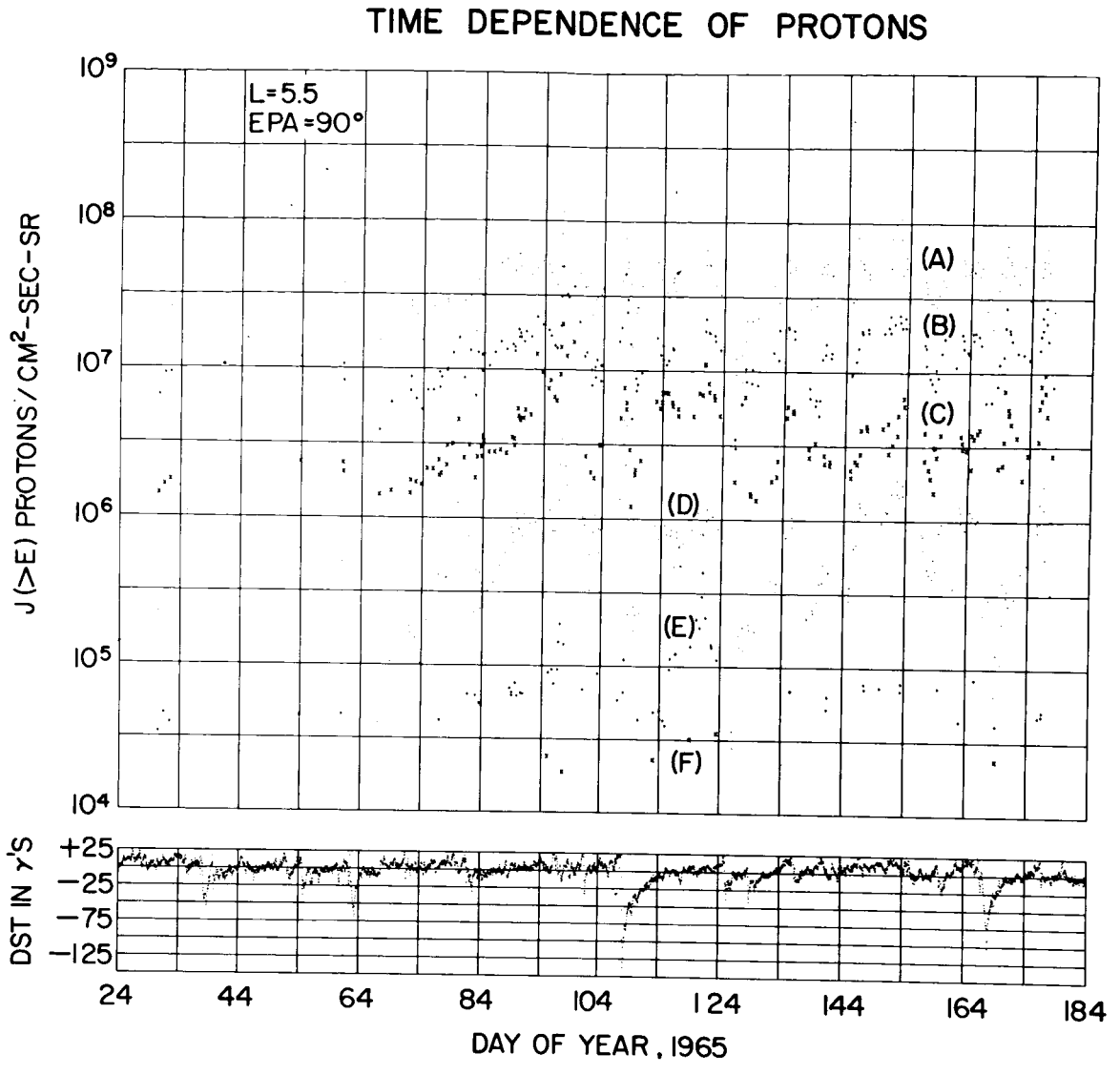

Figure 10. The time behavior of protons mirroring at the equator for six integral energies measured at L = 5.5. The different curves are marked with letters running from A to F corresponding to the energies 98, 134, 180, 345, 513, and 775 keV. The curves are displaced in order to avoid overlap and the values read from the curves A to F must be multiplied by 10 raised to the following exponents -1, -0.75, -0.50, -0.25, 0.0, and 0.25 in order to get the integral proton intensity above a certain energy in protons/cm^2 sec sr. Below the proton data are plotted the hourly average Dst values.

Table 3 shows values of the partial correlation coefficients R (between log J (> E) and Dst), together with values of the regression coefficient B_2, calculated for the time period beginning at day 114 of 1965 and ending at day 164. B_2 gives the change in the log intensity for a 1000 gamma change in Dst. We see that the variations with Dst in the particle intensity mirroring at the equator tends to increase with increasing L-value. The partial correlation coefficient is fairly high and significant. We will show that most of these variations are due to adiabatic changes in the particle fluxes. By this we mean, that the particles measured

Table 3

Regression coefficients (B_2) of proton intensity on Dst together with the corresponding partial correlation coefficient R during the days 114 to 164 of 1965. The values in Column I refer to the uncorrected data and the values in Column II corresponds to results obtained after the fluxes were corrected for adiabatic effects. The unit of B_2 is log 10 (protons/cm ^{2} s. sr)/1000 gamma.

L-Value	B_2		R		Energy (keV)
	I	II	I	II	
2.0	0.97 ± 0.2		0.24		134
2.5	1.20 ± 0.2	0.16 ± 0.2	0.27	0.04	"
3.0	1.66 ± 0.2	0.06 ± 0.2	0.43	0.02	"
3.5	3.37 ± 0.3	0.76 ± 0.3	0.62	0.18	"
4.0	4.45 ± 0.3	1.09 ± 0.3	0.70	0.25	"
4.5	5.02 ± 0.3	1.35 ± 0.3	0.71	0.30	"
5.0	6.03 ± 0.4	2.84 ± 0.4	0.70	0.43	"
2.0	1.02 ± 0.2		0.29		345
2.5	1.12 ± 0.2	-0.28 ± 0.2	0.26	0.08	"
3.0	1.66 ± 0.2	-0.02	0.39	0.01	"
3.5	4.08 ± 0.3	0.37 ± 0.4	0.64	0.08	"
4.0	7.06 ± 0.4	0.78 ± 0.4	0.77	0.14	"
4.5	8.04 ± 0.5	2.07 ± 0.5	0.77	0.32	"
5.0	8.21 ± 0.6	4.40 ± 0.6	0.70	0.53	"

respond to changes in the magnetic field conserving their three adiabatic invariants of motion.

2. Between day 29 and day 107 of 1965 the proton fluxes had fairly constant values below L = 4. There is though a slight increase in the fluxes above L = 3.5 and a similar decrease in the fluxes below this L-value. A model which can explain this kind of behavior would obviously be one where source and sink processes were nearly equal or the time constant for changes were very long compared with the time-period considered.

3. In the region $L \geq 4$ there is a larger variability in the fluxes. The fluxes exhibit both adiabatic changes which vary directly with the magnetic field (Dst) and non-adiabatic changes which do not track the field. In particular there is an irreversible build-up of the proton fluxes approximately between day 74 and 97 of 1965. This build-up affects L-values equal to 4.5 and above and it is most pronounced in the energy range 345 keV to 513 keV. This time-period is characterized by a below normal polar sub-storm activity as indicated by the Auroral Electrojet (AE) magnetic index (Davis and Sugiura, 1966) computed by Fairfield (private communication).

4. During magnetic storms the proton fluxes change irreversibly. Protons having energies less than about 200 keV were enhanced by as much as a factor of four while higher energy protons were depleted by as much as a factor of ten. The larger the storm main phase the deeper this process penetrated into the magnetosphere.

5. After the rapid storm-time changes have taken place, the particle fluxes tend to restore themselves back to the pre-storm value. The intensity of the low energy protons, which were enhanced, decreases and the intensity of the high energy ones, which were depleted, increases. The recovery rates increases with increasing L-value. A clear example of this kind of behavior is seen after the magnetic storm on day 107 of 1965, i.e. the April 18 geomagnetic storm.

Figures 11 through 16 show similar time plots of the pitch angle distribution as given by A_2, the slope of the long intensity curve plotted versus $\cos^2$ EPA. The most striking features of these plots are:

1. At all L-values there are variations in A_2 which exhibit correlations with variations in Dst. Some of the variations seem to track the field, while others do not show this behavior. The variability in the pitch angle distribution increases with increasing L-value. It is reasonable

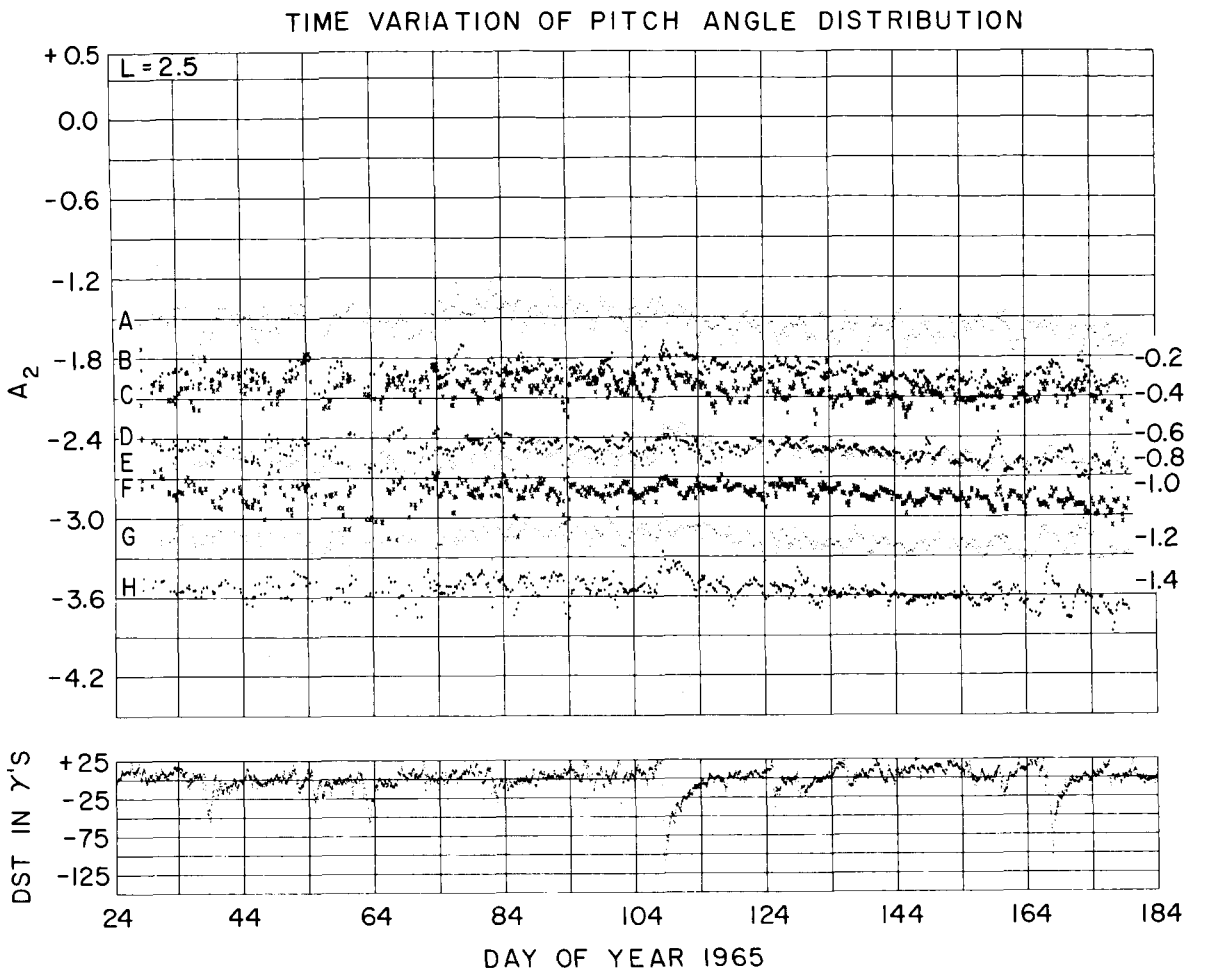

Figure 11. This figure shows the time behavior of the pitch angle distribution as given by A_2, the slope of the log intensity curve vs. $\cos^2$ EPA. The different curves are marked with letters running from A to H corresponding to the energies 98, 134, 180, 345, 513, 775, 1400 and 1700 keV. The numbers on the right-hand side indicate how much the different curves have been displaced in order to avoid overlap. Below are plotted the hourly average Dst values.

to assume that some of the variations in the pitch angle distribution are due to the particles responding in an adiabatic way to the field changes. We will however not test this, since it requires a two dimensional model of the field distortion.

2. At L = 2.5 the average values of A_2 are fairly constant. Above this L-value there is a decrease in A_2 from day 24 and up to day 74 of 1965. This means that during this time-period the pitch angle distribution tended to become more anisotropic. There was a steady loss of protons with pitch angles less than 90° while the intensity at 90° stayed constant

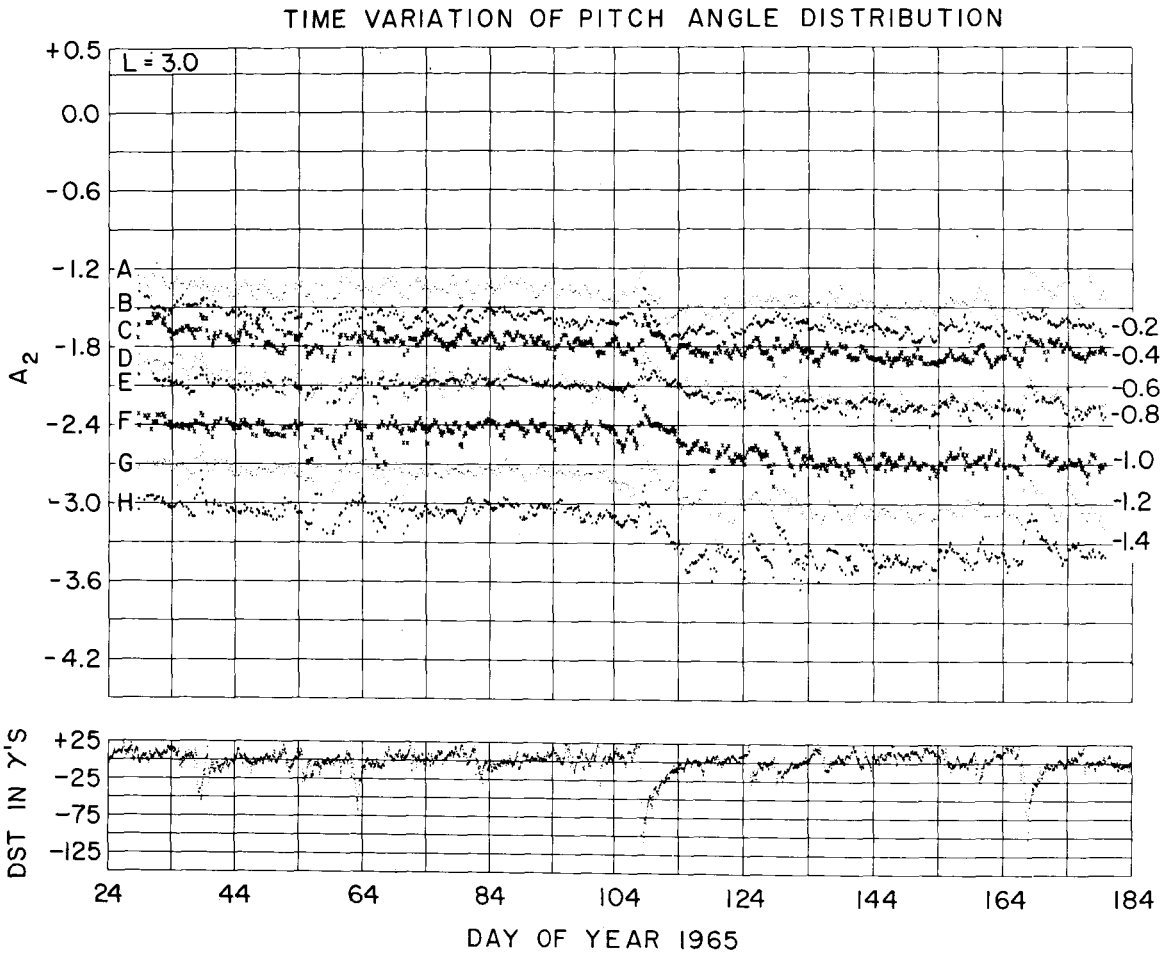

Figure 12. This figure shows the time behavior of the pitch angle distribution as given by A_2, the slope of the log intensity curve vs. $\cos^2$ EPA. The different curves are marked with letters running from A to H corresponding to the energies 98, 134, 180, 345, 513, 775, 1140 and 1700 keV. The numbers on the right-hand side indicate how much the different curves have been displaced in order to avoid overlap. Below are plotted the hourly average Dst values.

as seen in Figures 5 to 7. From day 74 and up to day 107 (the April 18 storm) the pitch angle distribution stayed more constant indicating either a reduced loss-rate of particles mirroring off the equator or an increased injection rate. This time-period is roughly the same time-period when there was a build-up of the fluxes mirroring at the equator in the energy range 345 keV to 513 keV, possibly due to decreased substorm activity.

3. During magnetic storms the pitch angle distribution changes irreversibly. At high L-values it becomes more isotropic and at low L-values it

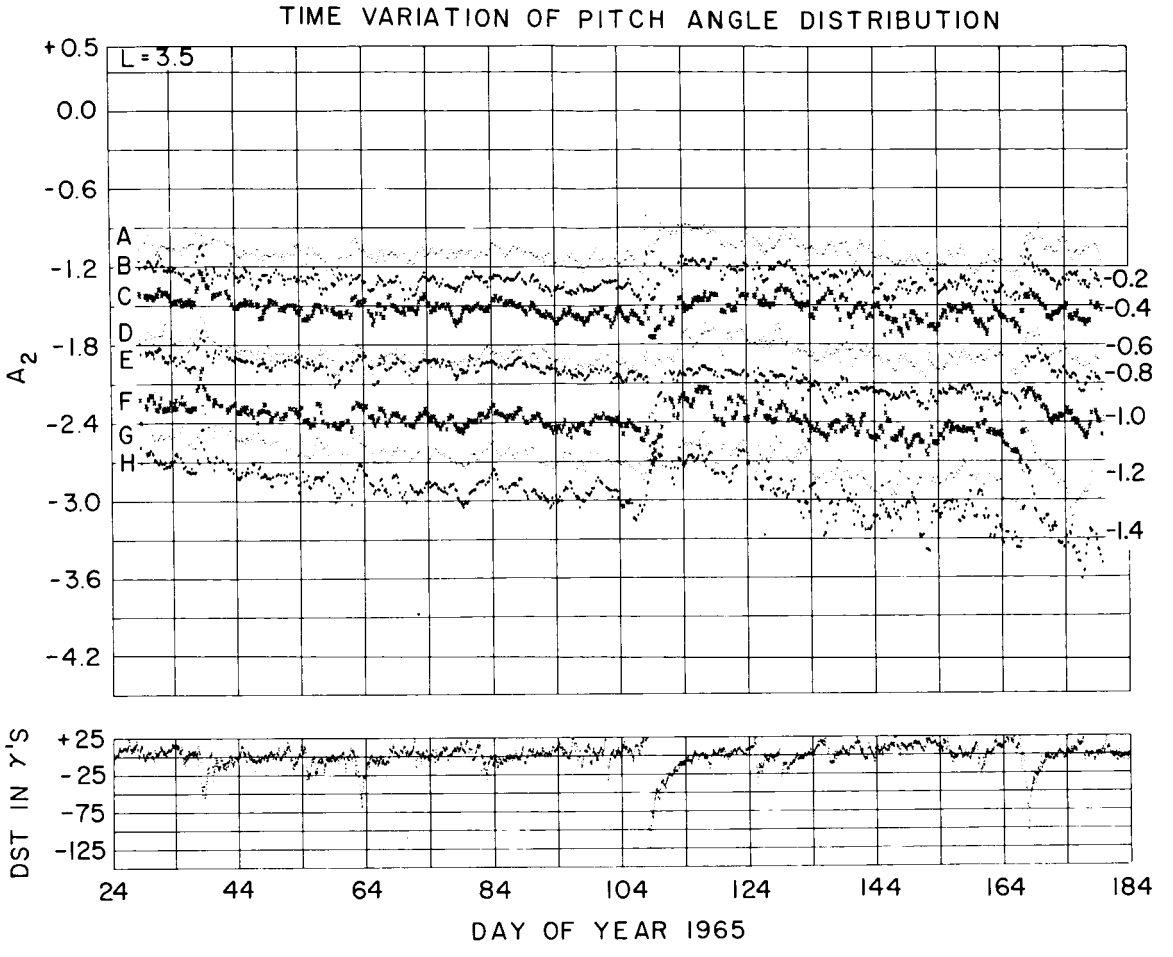

Figure 13. This figure shows the time behavior of the pitch angle distribution as given by A_2, the slope of the log intensity curve vs. $\cos^2$ EPA. The different curves are marked with letters running from A to H corresponding to the energies 98, 134, 180, 345, 513, 775, 1140 and 1700 keV. The numbers on the right-hand side indicate how much the different curves have been displaced in order to avoid overlap. Below are plotted the hourly average Dst values.

becomes more anisotropic than before the storm. This change in the pitch angle distribution penetrated deeper into the magnetosphere as the size of the storm increases. On the April 18 storm the changes in the pitch angle distribution corresponded to an injection of particles at pitch angles less than 90° above L = 3.5 and below this region to a loss of particles. For the June 15 (day 168) storm the change was to a more anisotropic pitch angle distribution in the region L = 3 through L = 4.0 and above this region it changed to a more isotropic one.

4. After the April 18 storm, the pitch angle distribution stays nearly isotropic with very little change for about 15 days. Then a remarkable

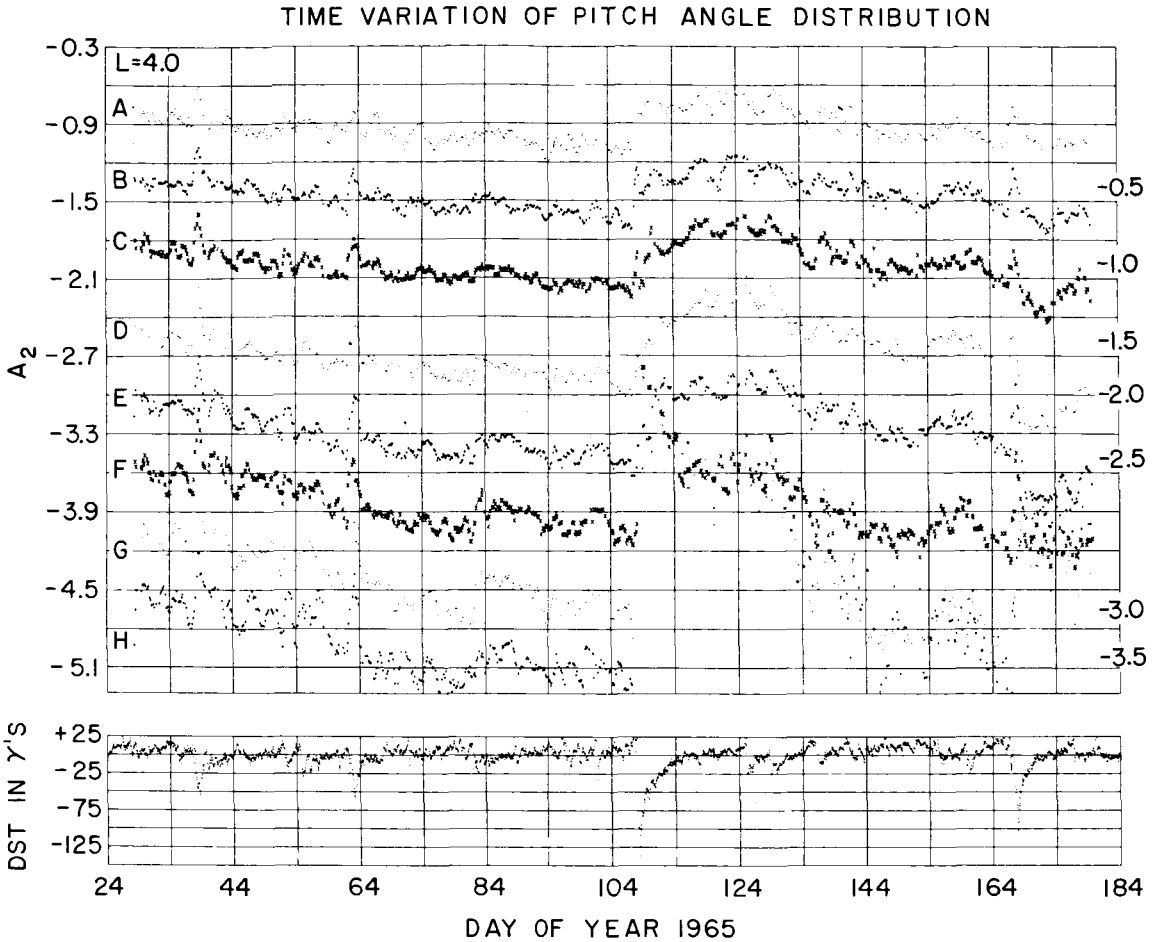

Figure 14. This figure shows the time behavior of the pitch angle distribution as given by A_2, the slope of the log intensity curve vs. $\cos^2$ EPA. The different curves are marked with letters running from A to H corresponding to the energies 98, 134, 180, 345, 513, 775, 1140 and 1700 keV. The numbers on the right-hand side indicate how much the different curves have been displaced in order to avoid overlap. Below are plotted the hourly average Dst values.

change in the pitch angle distribution can be seen at L = 4.5 and L = 5.0 on day 124 occurring simultaneously with a small magnetic storm. At that time the pitch angle distribution suddenly changes to a more anisotropic one. As can be seen the change is faster at high L-values than at low. In this particular event there is a great and rapid loss of particles with pitch angles less than 90° while there are almost no changes in particle intensities mirroring at the equator as may be seen in Figure 8 and 9 and more clearly in Figures 23 and 24 which, as will be discussed; show the intensities corrected for adiabatic effects.

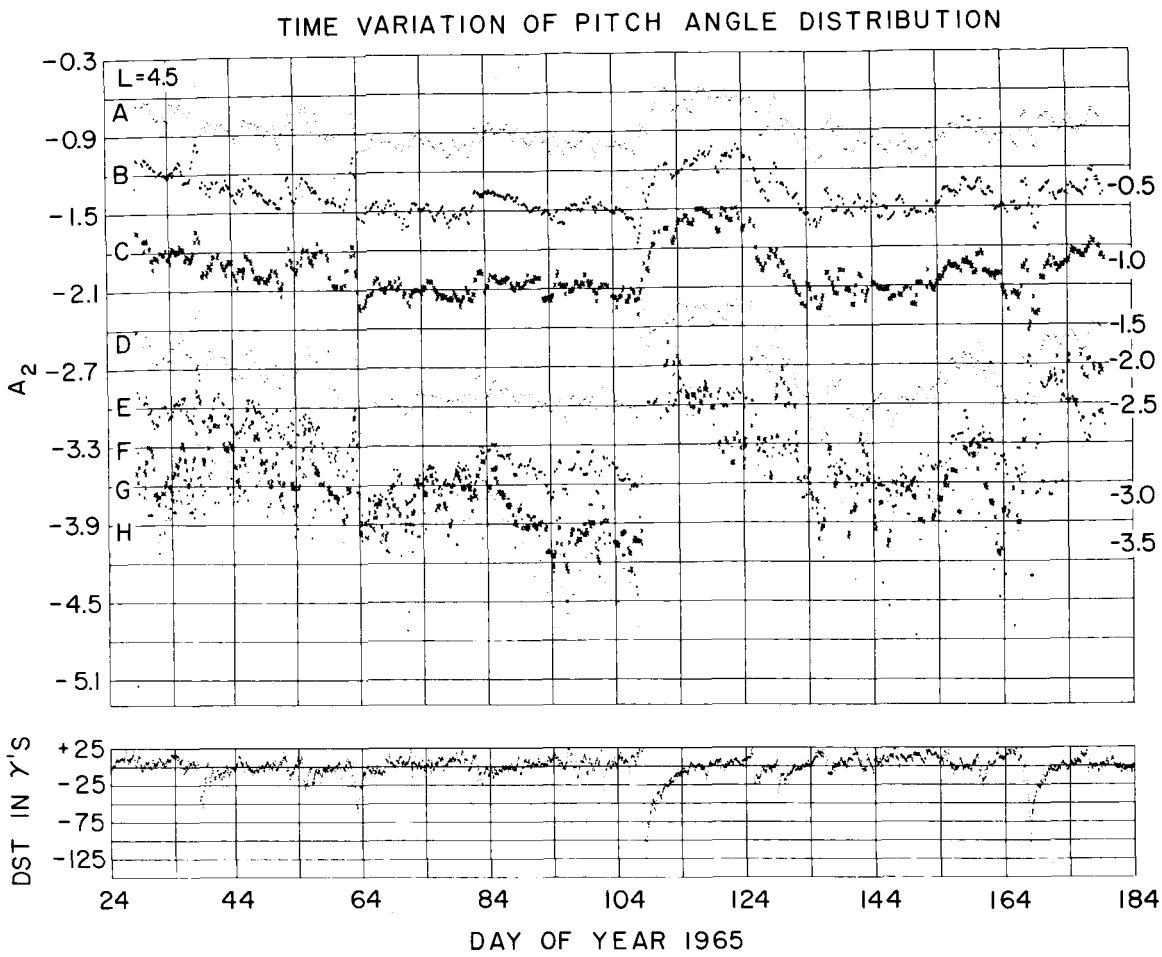

Figure 15. This figure shows the time behavior of the pitch angle distribution as given by A_2, the slope of the log intensity curve vs. $\cos^2$ EPA. The different curves are marked with letters running from A to H corresponding to the energies 98, 134, 180, 345, 513, 775, 1140 and 1700 keV. The numbers on the right-hand side indicate how much the different curves have been displaced in order to avoid overlap. Below are plotted the hourly average Dst values.

CALCULATED RING CURRENT EFFECTS ON THE TRAPPED PARTICLES

Any change in the geomagnetic field moves geomagnetically trapped particles in both position and energy. If the field changes are slow enough in both time and space the particles move in energy and position along trajectories that conserve the three adiabatic invariants of particle motion;

$$\mu = \frac{E_\perp}{B} \tag{9}$$

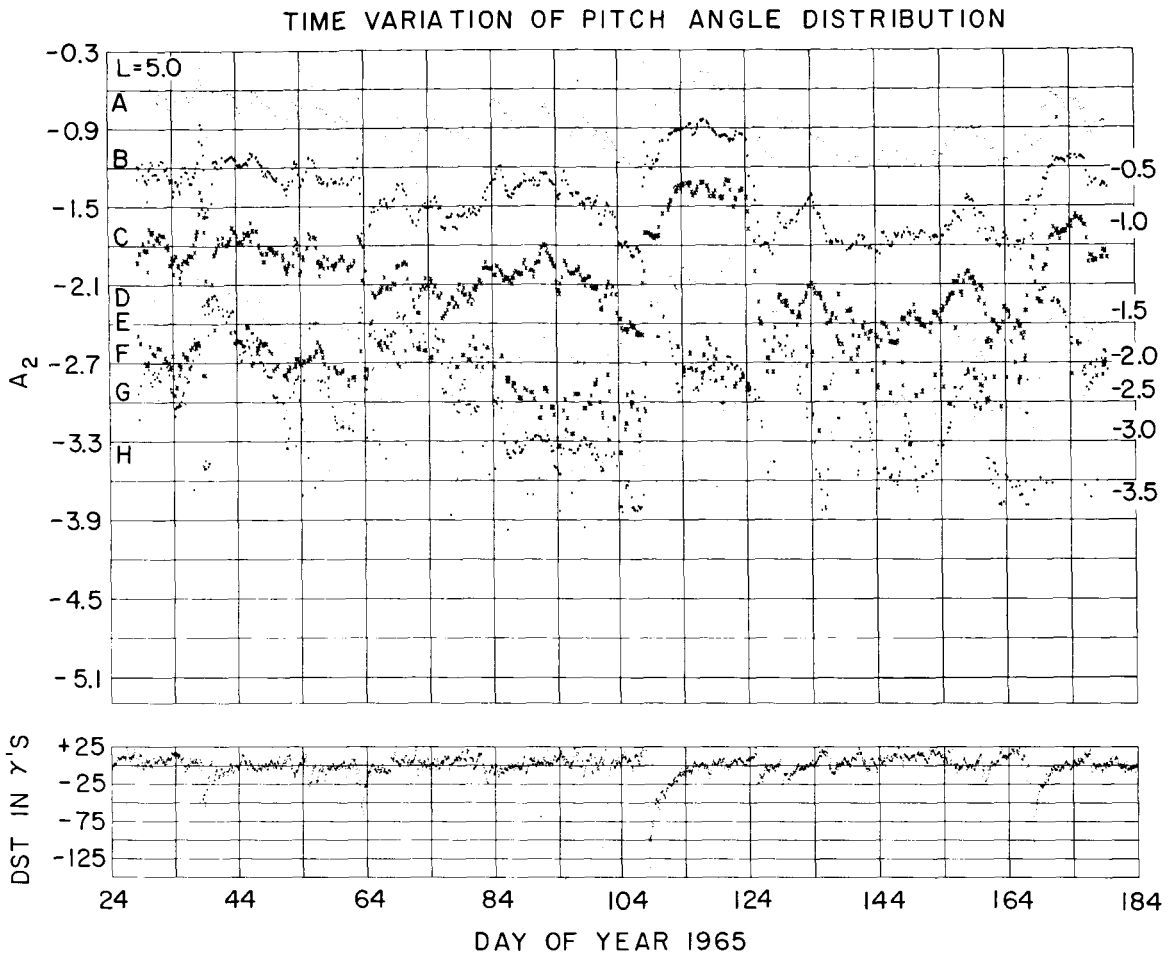

Figure 16. This figure shows the time behavior of the pitch angle distribution as given by A_2, the slope of the log intensity curve vs. $\cos^2$ EPA. The different curves are marked with letters running from A to H corresponding to the energies 98, 134, 180, 345, 513, 775, 1140 and 1700 keV. The numbers on the right-hand side indicate how much the different curves have been displaced in order to avoid overlap. Below are plotted the hourly average Dst values.

the first invariant or magnetic moment, where $E_\perp$ is particle energy perpendicular to the magnetic field and B is the magnetic field strength,

$$J = \oint m v_\parallel \, dS \tag{10}$$

the 2nd invariant or integral invariant, where m is the particle mass, $v_{||}$ is its velocity parallel to magnetic field, S is measured along the field and the integration is over a complete north-south oscillation,

$$\Phi = \int \mathbf{B} \cdot \mathbf{n}\, dA \tag{11}$$

the 3rd or flux invariant, where **B** is the vector field, **n** is the unit vector normal to the surface, A is surface area, and the integral is over any surface bounded by the drift path of the particle. Such a process is reversible, when the field restores, the particles return to their original energies and positions. Following McIlwain (1966a) we will call this type of particle motion adiabatic.

More rapid magnetic field fluctuations and electric fields can cause the particles to move along trajectories for which one or more of the adiabatic invariants are not conserved, i.e. non-adiabatic motion.

Liouville's Theorem applies in either case and states that the density in phase space δ remains constant along the particle trajectories and that $j = p^2 \delta$ where j is the differential directional intensity of particles and p is the particle momentum.

Thus one may use measurements obtained during periods when the geomagnetic field is changing to test whether particle motions are adiabatic or non-adiabatic by plotting j/p^2 as a function of time for fixed values of the three invariants evaluated for the actual field present during each measurement. If no time variation is observed the results are at least consistent with adiabatic motion. If time variations occur one must conclude that non-adiabatic motions or processes have taken place.

An alternative way of presenting the data is to transform the measured energy and position intensity distributions from the actual field to a reference field in such a way as to conserve the three invariants and δ, and plot the transformed intensity at a fixed location in the reference field and fixed transformed energy. The presence or absence of time variations have the same implications as above. This is the approach we have chosen to use.

In the following we will find expressions which show how A_1 in Equation (7), the log intensity of protons mirroring at the equator, transforms through such a process. Since for these particles the second invariant is zero only conservation of μ, Φ, and δ are needed to define the transformation.

We assume that the time dependent field is composed at a fixed dipole term and a time and L dependent disturbance field. We further assume that the disturbance field is symmetrical in the equatorial plane and directed perpendicular to this plane. The dipole term will then be used as the reference field.

For a dipole field with a dipole moment of -M (where the minus sign corresponds to the earth's southward directed dipole moment), the magnetic field on the equator at an equatorial radius of R_1 is given by

$$B_1 = M/R_1^3 \tag{12}$$

and the magnetic flux inside R_1 is given by

$$\phi_1 = -2\pi \int_{R_1}^{\infty} \frac{M}{r^3}\, r\, dr = -2\pi\, M/R_1 \tag{13}$$

For a dipole field plus a field $\Delta B(r)$, the magnetic field at an equatorial radius of R_2 is given by

$$B_2 = M/R_2^3 + \Delta B(R_2) \tag{14}$$

The magnetic flux inside R_2 is given by

$$\phi_2 = -2\pi\, M/R_2 + 2\pi \int_0^{R_2} \Delta B(r)\, r\, dr \tag{15}$$

If R_1 and R_2 correspond to the location of a given particle mirroring at the equator before and after the creation of the disturbance field, then conservation of the flux invariant demands that $\phi_1 = \phi_2$, thus

$$\frac{M}{R_1} = \frac{M}{R_2} - \int_0^{R_2} \Delta B(r)\, r\, dr \tag{16}$$

This equation gives us a relation of the position R_1 of the particle before the build up of the disturbance field and its position R_2 after the build up is completed assuming we know $\Delta B(r)$.

Now let $j_1(E, R)\,dE$ be the directional intensity within dE measured perpendicular to the magnetic field without any disturbance field. Liouville's Theorem states that the density in phase space δ remains constant during the movement of the particle from p_1, R_1, to p_2, R_2 and that $j(E, R) = p^2 \delta$ where p is the momentum of the particle. By this we are able to relate the measured integral intensities with and without the presence of the disturbance magnetic field.

$$j_1(E_1, R_1)/E_1 = j_2(E_2, R_2)/E_2 \tag{17}$$

conservation of the first adiabatic invariants gives

$$E_1/E_2 = B_1/B_2 \tag{18}$$

Evaluating for integral intensities

$$J_2(>E_2, R_2) = \int_{E_2}^{\alpha} E_2\, j_2(E_2^1, R_2)\, dE_2^1 \tag{19}$$

and changing the variable to E_1^1 we get from (18)

$$dE_2^1 = B_2/B_1\, dE_1^1 \tag{20}$$

substitute this in Equation (19) and using (17) we get

$$J_2(>E_2, R_2) = \left(\frac{B_2}{B_1}\right)^2 \int_{E_3}^{\alpha} j_1(E_1^1, R_1)\, dE_1^1 = \left(\frac{B_2}{B_1}\right)^2 J_1\left(>E_2\frac{B_1}{B_2}, R_2 - \Delta R\right) \tag{21}$$

where $E_3 = E_2 \cdot B_1/B_2$. $\Delta R = R_2 - R_1$ can be found from Equation (16) and B_1 and B_2 are given respectively by Equations (12) and (14).

By taking the logarithm of Equation (21) and comparing it with Equation (7) we obtain the desired relation for transforming A_1 the log intensity of particles mirroring at the equator in the disturbed field, to its value in the reference field A_1^*.

$$A_1^*(>E_2, R_2) = 2 \cdot \log\left(\frac{B_1}{B_2}\right) + A_1\left(>E_2 \cdot \frac{B_1}{B_2}, R_2 - \Delta R\right) \qquad (22)$$

The model disturbance field used in our calculation is given by the following expression

$$\Delta B(r) = C \cdot Dst \cdot f(r) + B_{ind}(r) \qquad (23)$$

where r is the radial distance from the earth center and $f(r)$ gives the radial dependence of the ringcurrent magnetic field. C and $B_{ind}(r)$ are factors taking into account the field created by currents induced in the earth.

The function $f(r)$ used in the calculations is shown in Figure 17. It is based on; (1) the values measured by Cahill (1966) on Explorer 26 during the outbound pass of orbit number 376, 19 April 1965, for the region 3.2 to 5.0 earth radii, (2) the Dst value at the time of the pass, and (3) a model calculated by Hoffman and Bracken (1967) for the region above 5 earth radii. Since the shape of the disturbance field curve is time dependent, as shown by Cahill's results, and probably varies from one storm to another, it would be better to use measured values on each pass. However the measured values were not available when the study began.

The magnitude of C depends on the frequency of the time variations in the ringcurrent field. Takeuchi and Saito (1963) have computed that C varies from 0.703 to 0.735 when the period of the disturbance field changes from 3 min to 3 days. We need to know how C varies for longer periods in order to make the proper adiabatic corrections to the measured proton intensities. In what follows values of C for variations having periods greater than 3 days will be determined. $\Delta B(r)$ is derivable from a magnetic scaler potential Ω in the region where there is no true currents. If the ringcurrent field contains time only in the factor $\exp(iwt)$ then following Chapman and Price (1930) we can

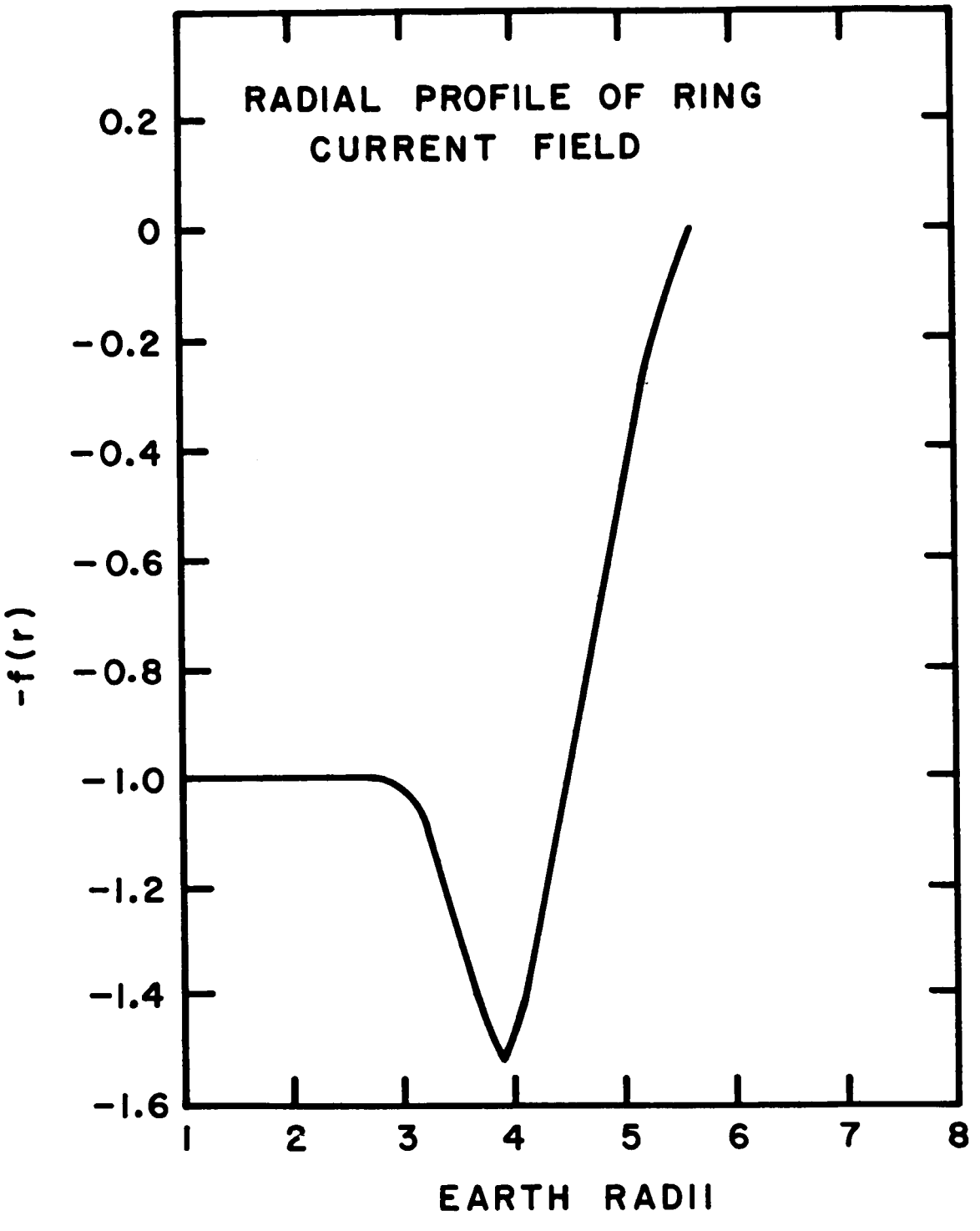

Figure 17. The radial dependence of the ringcurrent magnetic field used in the model calculation of adiabatic effects on the trapped protons.

write

$$\Omega = a \sum_{m=1}^{\infty} \left(E_m \left(\frac{r}{a}\right)^m + I_m \left(\frac{r}{a}\right)^{-m-1} \right) \exp(iwt)\, P_m(\cos\theta) \qquad (24)$$

where a is the radius of the earth and θ is the angle between the earth's dipole axis and the r-vector. P_m is the Legendre Polynomial of order m. E_m is associated with the part of the potential that has its origin above the earth's surface, while I_m is associated with the part that originated within the earth.

The field $\Delta B(r)$ outside the region where true currents are flowing can then be expressed as

$$\Delta B(r) = -\frac{1}{r}\frac{\partial \Omega}{\partial \theta} = -\sum^{\infty} \left(E_m \left(\frac{r}{a}\right)^{m-1} + I_m \left(\frac{r}{a}\right)^{-m-2} \right)$$

$$\cdot \exp(iwt) \cdot \frac{\partial P_m}{\partial \theta} \quad m = 1, 3, 5 \qquad (25)$$

As our ringcurrent field is assumed symmetric with respect to the equatorial plane we need only consider harmonics of odd degree.

Chapman and Price (1930) shows that except during the initial ten hours of a magnetic storm, the field, near the earth, is adequately represented by the first harmonic term m = 1 and that even in the initial phase also is largely from the m = 1 term.

In the equatorial plane Equation (25) can be written assuming m = 1

$$\Delta B(r) = \left(E_1 + I_1 \left(\frac{r}{a}\right)^{-3} \right) \exp(iwt) \qquad (26)$$

and at the earth's surface (r = a) we have

$$\Delta B(a) = \left(E_1 + I_1\right) \exp(iwt) = E_1 \left(1 + S_1\right) \exp(iwt) \tag{27}$$

where

$$S_1 = \frac{I_1}{E_1}$$

The measured disturbance field at the earth's surface at the equator is given by Dst. From Equation (27) we have that

$$\Delta B(a) = Dst = E_1 \left(1 + S_1\right) \exp(iwt) \tag{28}$$

We can now express E_1 and I_1 in terms of Dst and S_1

$$E_1 = Dst \cdot \left[\left(1 + S_1\right) \cdot \exp(iwt)\right]^{-1} \tag{29}$$

$$I_1 = S_1 \cdot E_1 \tag{30}$$

Using this two expression we can rewrite Equation (26)

$$\Delta B(r) = \frac{Dst}{1 + S_1} + \frac{Dst}{1 + S_1} \cdot S_1 \cdot \left(\frac{r}{a}\right)^{-3} \tag{31}$$

Remembering that this equation is valid near the earth and that $f(r)$ is equal to one in this region we can compare Equation (31) with (23) and

identify C and B_{ind} as

$$C = \frac{1}{1 + S_1} \tag{32}$$

and

$$B_{ind} = \frac{S_1}{1 + S_1} \, Dst \left(\frac{r}{a}\right)^{-3} \tag{33}$$

Using these expressions for C and B_{ind} in Equation (23) we are now able to express the ringcurrent field in the whole region of interest knowing Dst and S_1. Dst is known from ground-based measurements and the ratio $S_1 = I_1/E_1$ is obtained by solving a non-linear first order differential equation Ekcardt (1963). The equation is solved for the electrical conductivity of the earth's mantle and crust as given by McDonald (1957) and for external field variations having different periods. The results of the calculations are given in Table 4.

As can be seen the value of C does not change much over a wide range of frequencies in the external field variations. This justifies us in using

Table 4

Calculated values real and imaginary parts of the ratio (S_1) between internal and external source coefficients of the magnetic scalar potential.

Period (Days)	Re (S_1)	Im (S_1)	C
0.5	0.404	0.0427	0.714
2.0	0.363	0.0483	0.735
13	0.305	0.0220	0.766
30	0.301	0.0100	0.769
180	0.300	0.0160	0.769

a constant value for C in our calculations. The imaginary part of C is much less than the real one which means that the ringcurrent field and Dst are approximately in phase with each other.

In our calculations we have used the value C = 0.7. Furthermore we have dropped the B_{ind} term in Equation (23) when evaluating Equations (14) and (16). That is we do not take into account the fields at R_2 and beyond produced by the induced earth currents and therefore the resulting values of B_2 and R_2 are in error. At two earth radii the error in B_2 amounts to 1/10 of the field due to the external ringcurrent and with Dst = -200γ the error in R_2 is .002 earth radii. Since these errors were small and fall off rapidly with increasing radial distance we are justified in dropping the term.

Using the recipe outlined we have taken each radial intensity profile of protons in the energy range 100 keV to 1700 keV as measured by Explorer 26 (two profiles each orbit) and transformed them to a field where Dst is zero, interpolating both in energy and L-value. The value of Dst used in the transformation equations is the value corresponding to the half orbit center time. In Figure 18 we show a radial profile measured on day 109 of 1965. The Dst value corresponding to the center time was -46γ. In this figure we also show the transformed profile corresponding to no disturbance field as calculated by the method outlined. A negative value of Dst, a build up of the ringcurrent, has the effect of pulling out field-lines, if the three adiabatic invariants of a particle motion are conserved the particle will follow the field line and as it moves outward its energy decreases (conservation of the first adiabatic invariant). Whether the particle intensity as seen by a threshold-detector fixed in space, increases, or decreases during such a process, depends on the gradients of the particles both in energy and r-space and also upon the value of B_2/B_1 entering into Equation (22).

Figures 19 to 24 show the time-variations for protons mirroring at the equator after the adiabatic transformation. It can be seen that variations in the proton intensities are much less dependent on variations in the magnetic field, as given by Dst, than the case was for the uncorrected data. In order to get a quantitative measure for this we perform a regression analysis of the transformed data using the function given in (8). These values of the regression coefficients are given in Table 3 where they can be compared with the corresponding coefficients obtained by analyzing the uncorrected data for the same time period.

As seen the adiabatic transformation reduces the regression coefficients of proton intensity on Dst by a factor of 5 and more out to L = 4.5 earth radii. Figure 25 shows plots against L of the regression coefficients calculated with

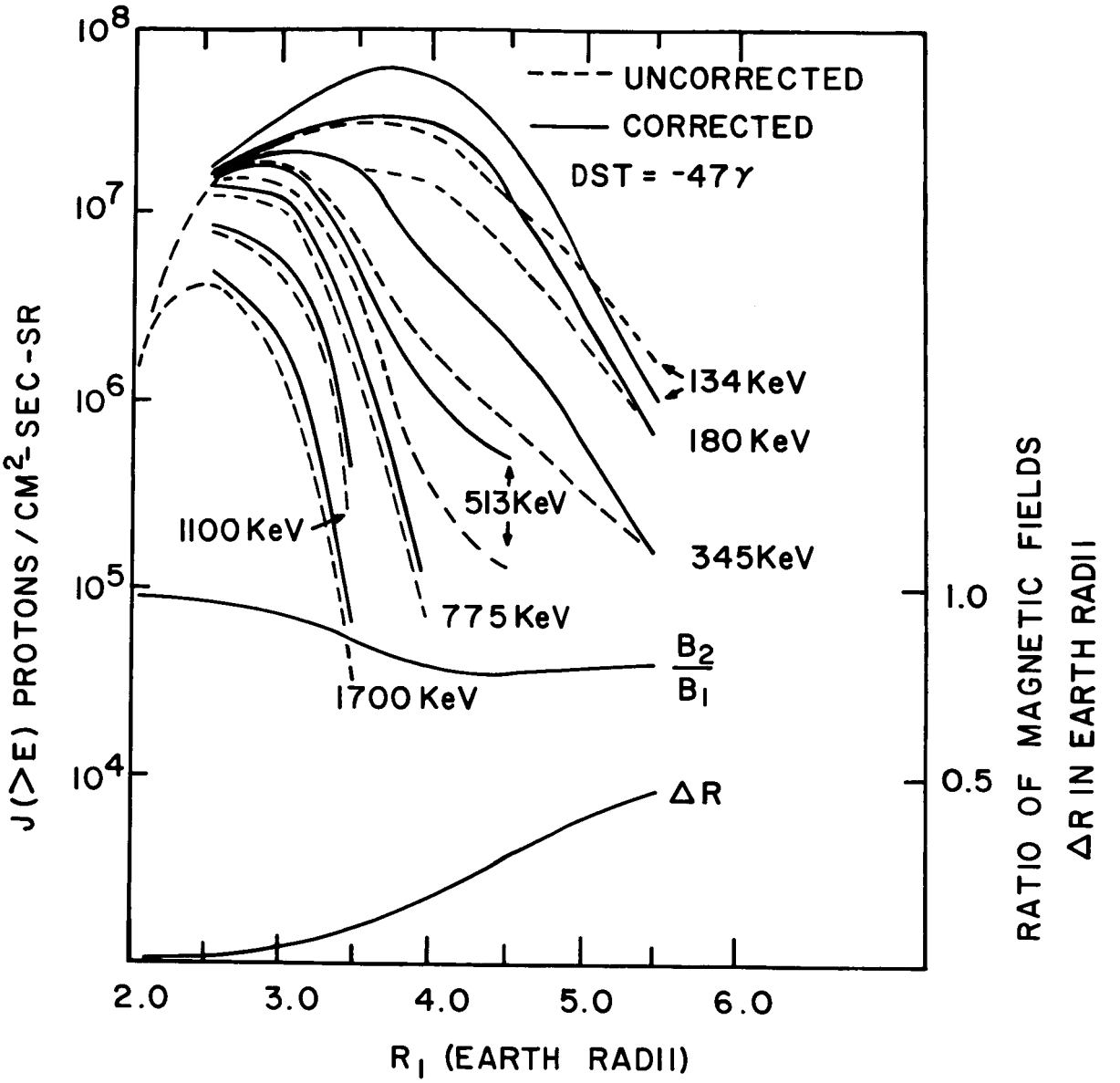

Figure 18. The radial proton integral energy intensity profile as measured on day 109 of 1965, when Dst = -46γ, together with the transformed profile corresponding to Dst = 0 assuming the three adiabatic invariants of motion conserved. The radial dependence of the ratio between the magnetic field after and before the build up of the ringcurrent and the radial movement ΔR of the particles are shown in the lower part of the figure.

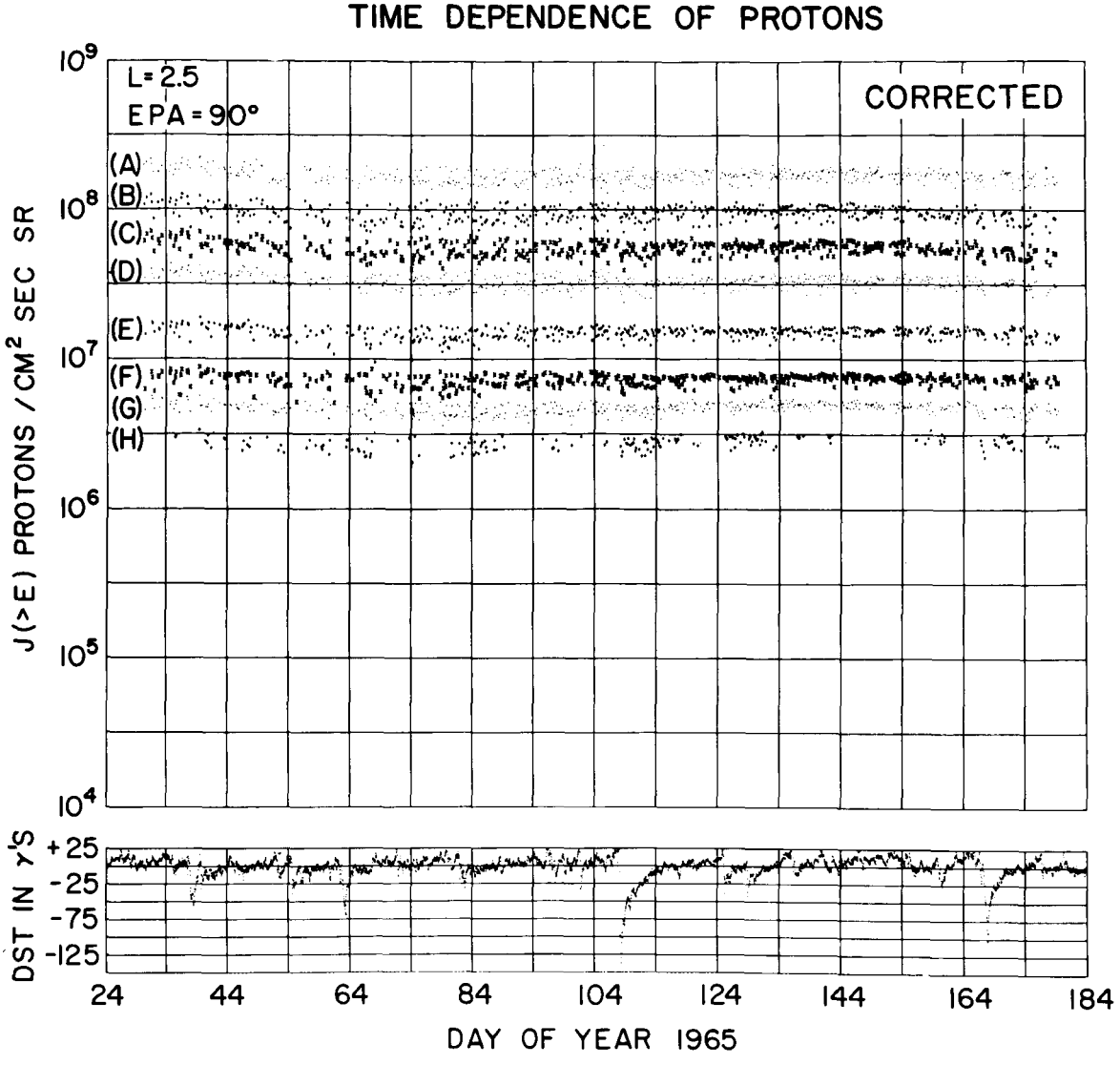

Figure 19. The time behavior of protons mirroring at the equator at L = 2.5 after the adiabatic effects are removed. The different curves are marked with letters running from A to H corresponding to the energies 134, 180, 220, 345, 513, 775, 1140 and 1700 keV. The curves are displaced in order to avoid overlap and the values read from the curves A to H must be multiplied by 10 raised to the following exponents -1, -0.75, -0.50, -0.25, 0.0, 0.25, 0.25 and 0.25 in order to get the integral proton intensities above a certain energy in protons/cm^2 sec sr. Below the proton data are plotted the hourly average Dst values.

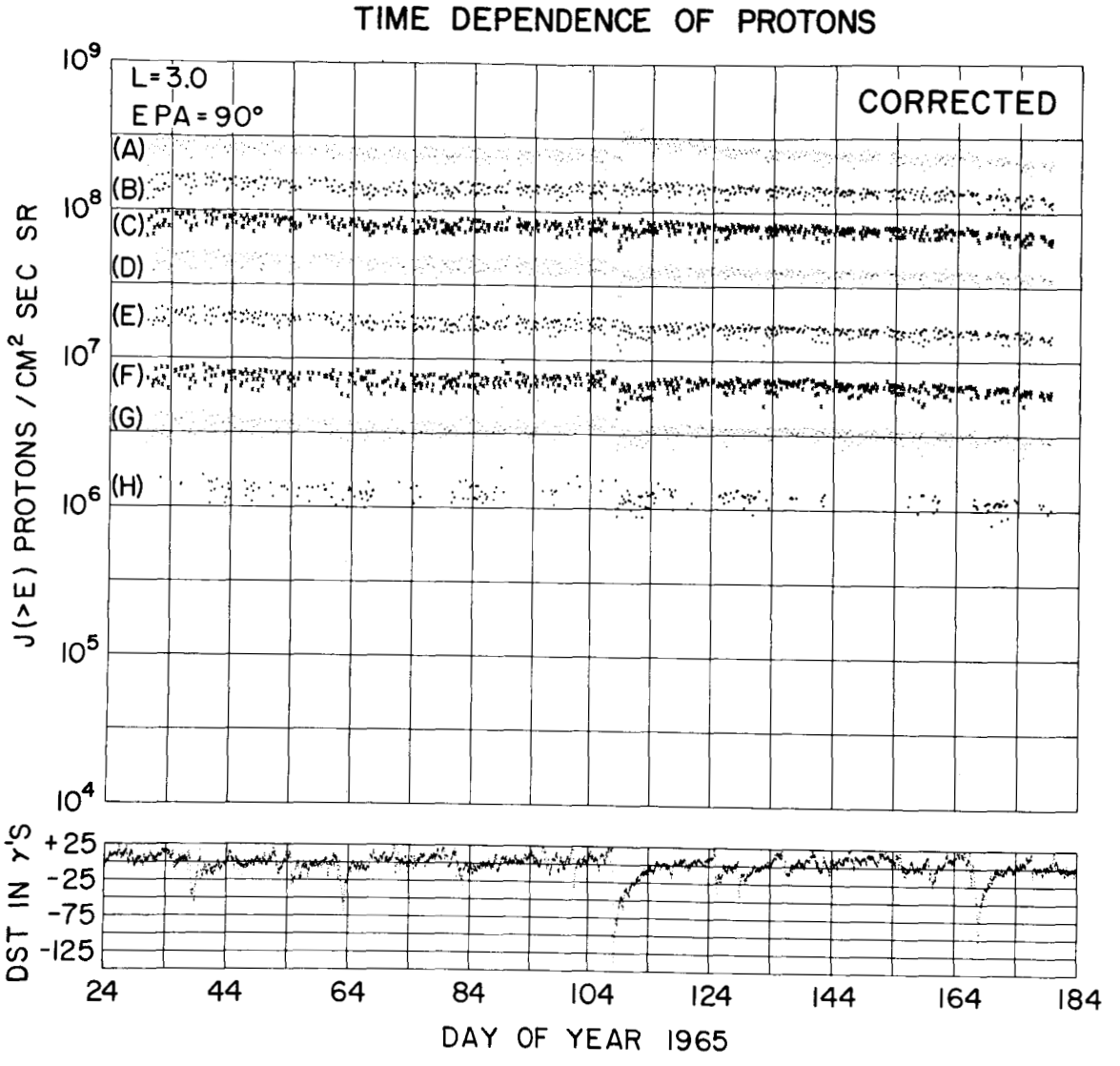

Figure 20. The time behavior of protons mirroring at the equator at L = 3.0 after the adiabatic effects are removed. The different curves are marked with letters running from A to H corresponding to the energies 134, 180, 220, 345, 513, 775, 1140 and 1700 keV. The curves are displaced in order to avoid overlap and the values read from the curves A to H must be multiplied by 10 raised to the following exponents -1, -0.75, -0.50, -0.25, 0.0, 0.25, 0.25 and 0.25 in order to get the integral proton intensities above a certain energy in protons/cm^2 sec sr. Below the proton data are plotted the hourly average Dst values.

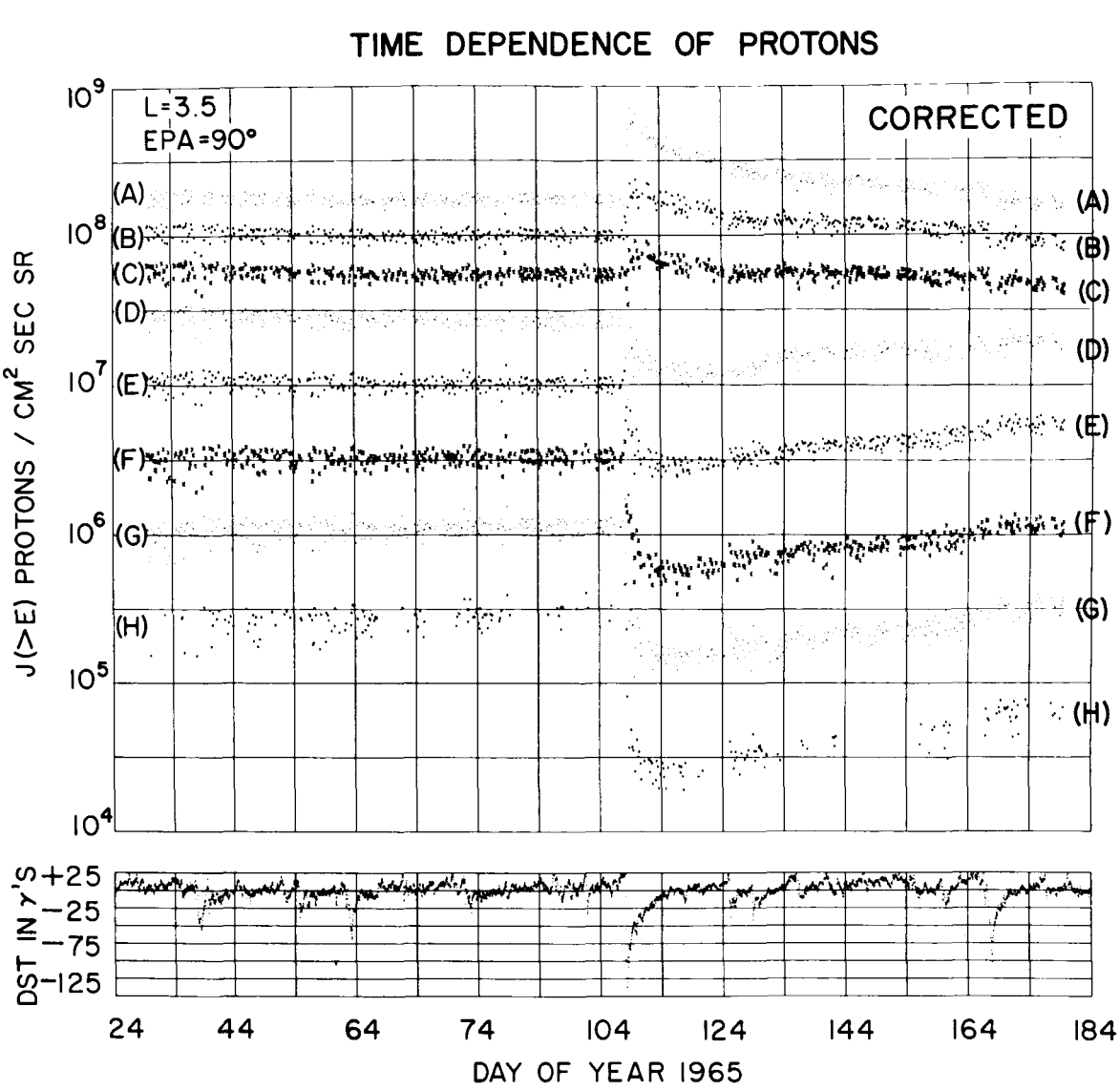

Figure 21. The time behavior of protons mirroring at the equator at L = 3.5 after the adiabatic effects are removed. The different curves are marked with letters running from A to H corresponding to the energies 134, 180, 220, 345, 513, 775, 1140 and 1700 keV. The curves are displaced in order to avoid overlap and the values read from the curves A to H must be multiplied by 10 raised to the following exponents -1, -0.75, -0.50, -0.25, 0.0, 0.25, 0.25 and 0.25 in order to get the integral proton intensities above a certain energy in protons/cm^2 sec sr. Below the proton data are plotted the hourly average Dst values.

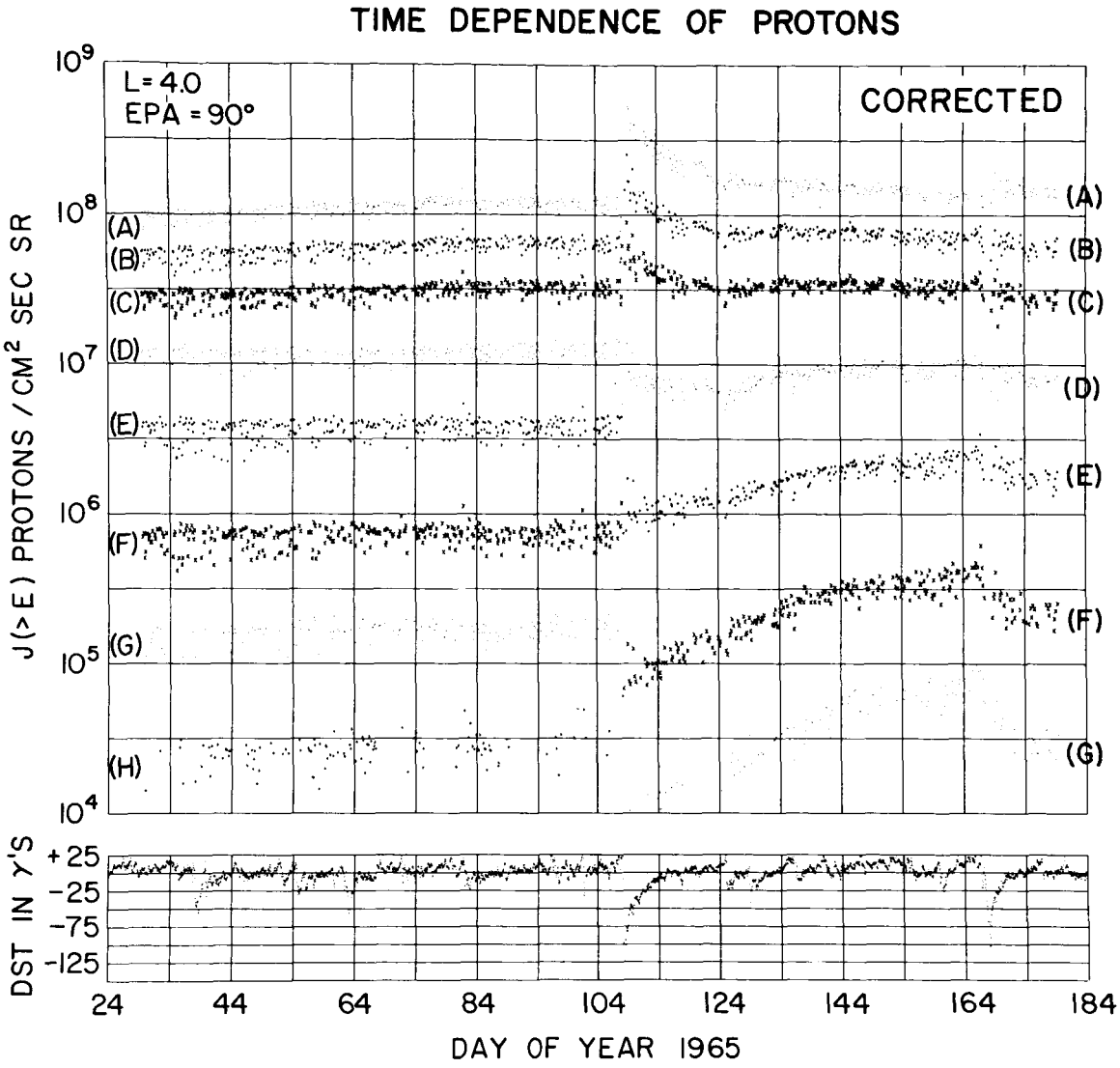

Figure 22. The time behavior of protons mirroring at the equator at L = 4.0 after the adiabatic effects are removed. The different curves are marked with letters running from A to G corresponding to the energies 134, 180, 220, 345, 513, 775, and 1140 keV. The curves are displaced in order to avoid overlap and the values read from the curves A to G must be multiplied by 10 raised to the following exponents -1, -0.75, -0.50, -0.25, 0.0, 0.25, and 0.25 in order to get the integral proton intensities above a certain energy in protons/cm^2 sec sr. Below the proton data are plotted the hourly average Dst values.

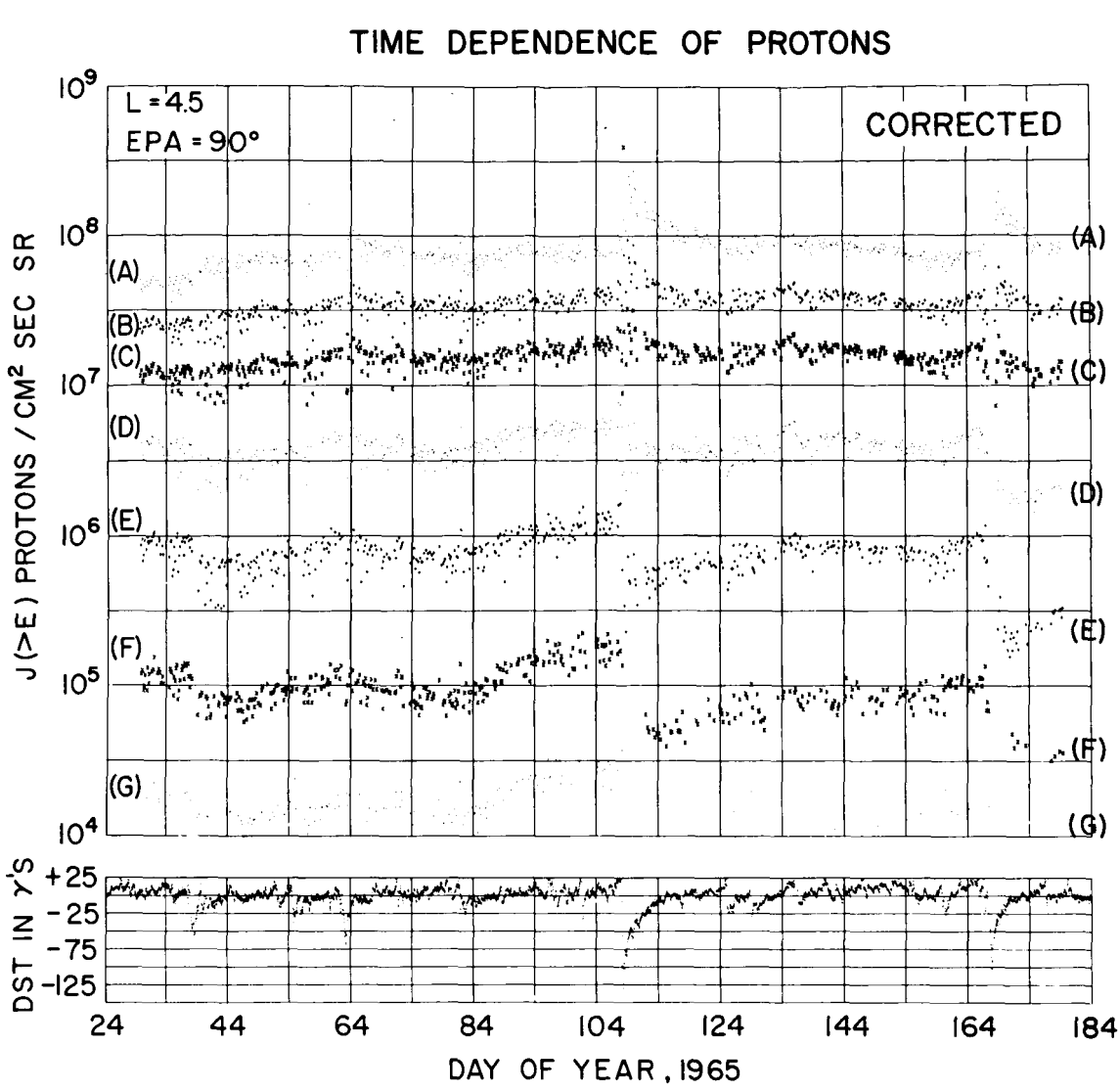

Figure 23. The time behavior of protons mirroring at the equator at L = 4.5 after the adiabatic effects are removed. The different curves are marked with letters running from A to G corresponding to the energies 134, 180, 220, 345, 513, 775, and 1140 keV. The curves are displaced in order to avoid overlap and the values read from the Curves A to G must be multiplied by 10 raised to the following exponents -1, -0.75, -0.50, -0.25, 0.0, 0.25, and 0.25 in order to get the integral proton intensities above a certain energy in protons/cm^2 sec sr. Below the proton data are plotted the hourly average Dst values.

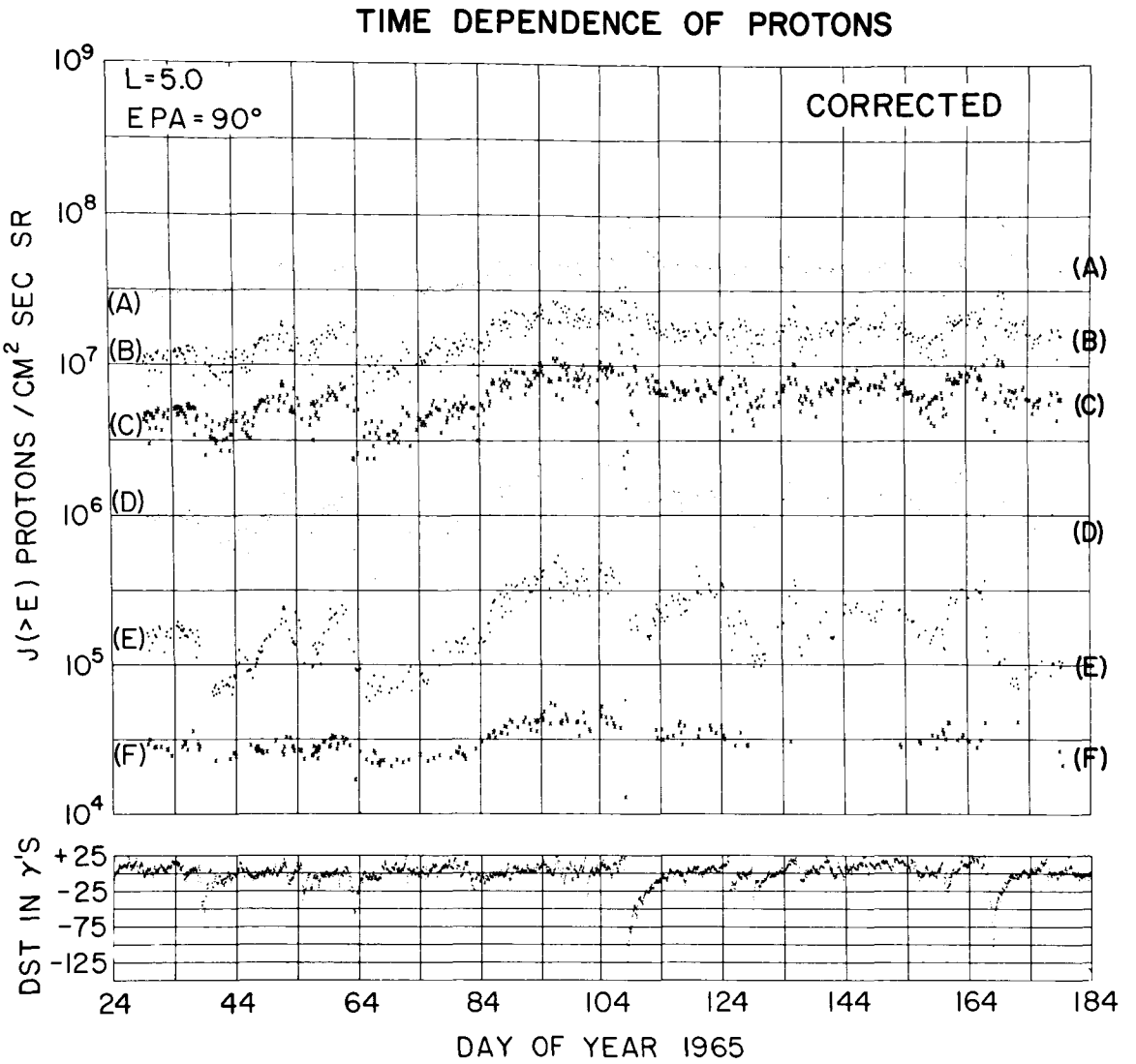

Figure 24. The time behavior of protons mirroring at the equator a L = 5.0 after the adiabatic effects are removed. The different curves are marked with letters running from A to F corresponding to the energies 134, 180, 220, 345, 513, and 775 keV. The curves are displaced in order to avoid overlap and the values read from the curves A to F must be multiplied by 10 raised to the following exponents -1, -0.75, -0.50, -0.25, 0.0, and 0.25 in order to get the integral proton intensities above a certain energy in protons/cm^2 sec sr. Below the proton data are plotted the hourly average Dst values.

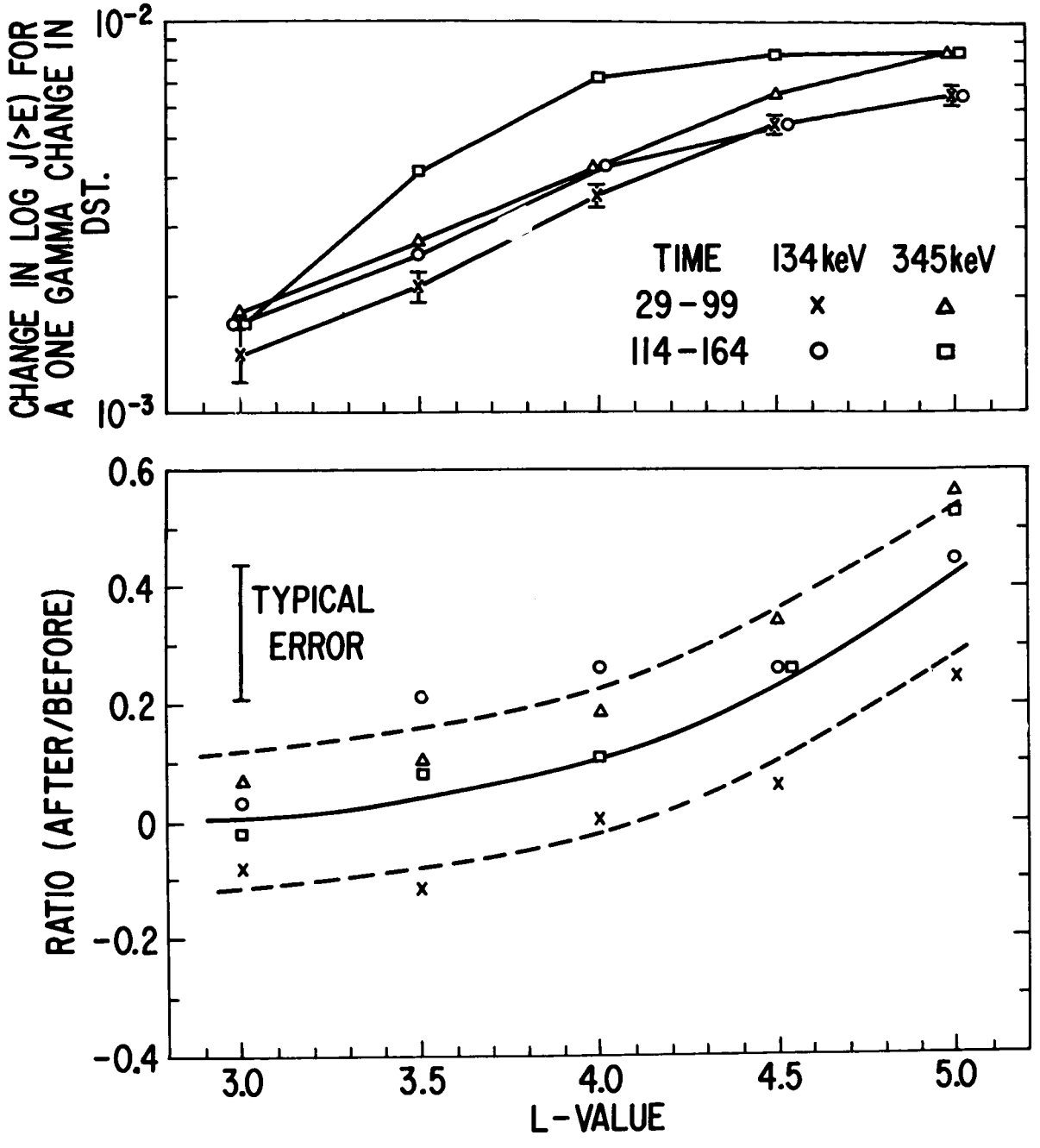

Figure 25. The regression coefficient of proton intensity on Dst vs. radial distance before the proton data are corrected for adiabatic variations. The lower part of the figure shows the ratio between the regression coefficients after and before the fluxes were corrected for adiabatic effects as a function of radial distance.

the uncorrected data and the ratio of the regression coefficients calculated with the transformed and untransformed data.

The transformed fluxes below L = 4 are now running very smoothly except for the times when there is a large magnetic activity. During these times large non-adiabatic effects take place. The transformed fluxes above L = 4 still show some variability correlated with Dst. These variations could be due to a number of things. (1) The simple model of the ringcurrent used, which we expect to have the least accuracy at high L-values. (2) At these high L-values possible adiabatic effects due to field changes caused by variations in the solar plasma pressure against the boundary of the magnetosphere and/or by changing tail field would be most pronounced. (3) Small magnetic disturbances as seen at the earth surface could have non-adiabatic effects at these high L-values. (4) There also is the possibility that variations seen at L = 4 and 4.5 could be due to a fast inward diffusion of changes at still higher L-values. One thing which makes it hard to differentiate adiabatic from non-adiabatic effects at these high L-values is that the time constant for the fluxes to recover after non-adiabatic effects, is comparable with the recovery time constant of Dst.

COMPUTATION OF THE RINGCURRENT FIELD FROM PARTICLE DATA

The fact that many fluctuations of trapped particle intensities are clearly caused by global changes in the earth's magnetic field, suggest the possibility to use the trapped particle measurements themselves to compute the variations in the magnetic field. Since particles respond to changes in the magnetic flux inside the magnetic shell upon which they are trapped, they are quite insensitive to the effect of ionospheric and induced earth currents which plague ground-based measurements. This method has been used by McIlwain (1966b) to compute Dst values from fluxes of 0.5 MeV electrons measured by the Explorer 15 satellite.

We assume as in the previous that the magnetic field can be expressed as the sum of a dipole term and a ringcurrent term. The ringcurrent field is given by Equation (23). B_{ind} is neglected for the reasons explained previously and $C \cdot Dst$ is replaced by an unknown parameter K. The ringcurrent field is then given by

$$\Delta B(r) = K \cdot f(r) \tag{34}$$

By changing the value of K the ringcurrent field will attain different values.

We now want to find the value of K which transform a particular radial integral energy intensity distribution into a reference distribution. The reference distribution is the radial integral energy intensity distribution measured if the ringcurrent field was zero. The reference distribution is obtained for the time period 108 to 170th day of 1965 from Equation (8) used on data not corrected for adiabatic variations and then putting Dst = 0. Equation (8) which is quadratic in time can account for long-term non-adiabatic effects, but not for abrupt changes taking place during a larger geomagnetic storm.

By using a general least square method the radial integral energy intensity distribution of protons mirroring at the equator measured during a particular half orbit is transformed into the reference distribution using the relations (12), (14), (16), and (22) substituting K for C · Dst in Equation (23). Data obtained at $L \leq 4$ were used.

The value of K obtained in this fitting process is the one which gives the best overall agreement between the reference distribution and the transformed distribution measured during a particular half orbit.

In Figure 26, K and Dst are plotted vs. time from day 107 to day 170 of 1965. It is seen that during this time interval the time variations in Dst and K tends to follow each other. It is interesting to study the linear correlation between K and Dst using the reation

$$K = A \cdot Dst + B \tag{35}$$

This is done for three time intervals during the time-period considered and the results of the computation are shown in Table 5.

The RMS is the standard deviation around the line. The linear correlation coefficient is fairly high and the value of B is close to zero which is what one should expect as the reference distribution corresponds to Dst = 0. Figure 27 shows K vs. Dst for the time period 149-170 day of 1965. Comparing Equation (23) and Equation (34) remembering that B_{ind} is neglected we get

$$K = C \cdot Dst \tag{36}$$

As the value of B in Equation (35) is approximately equal to zero, we have comparing Equation (35) and (36) that A = C. Now going back to Equation (32), and remembering that C is a factor taking into account the induced field created in the earth, we can see that A gives an estimate of $(1 + S_1)^{-1}$. This estimate of

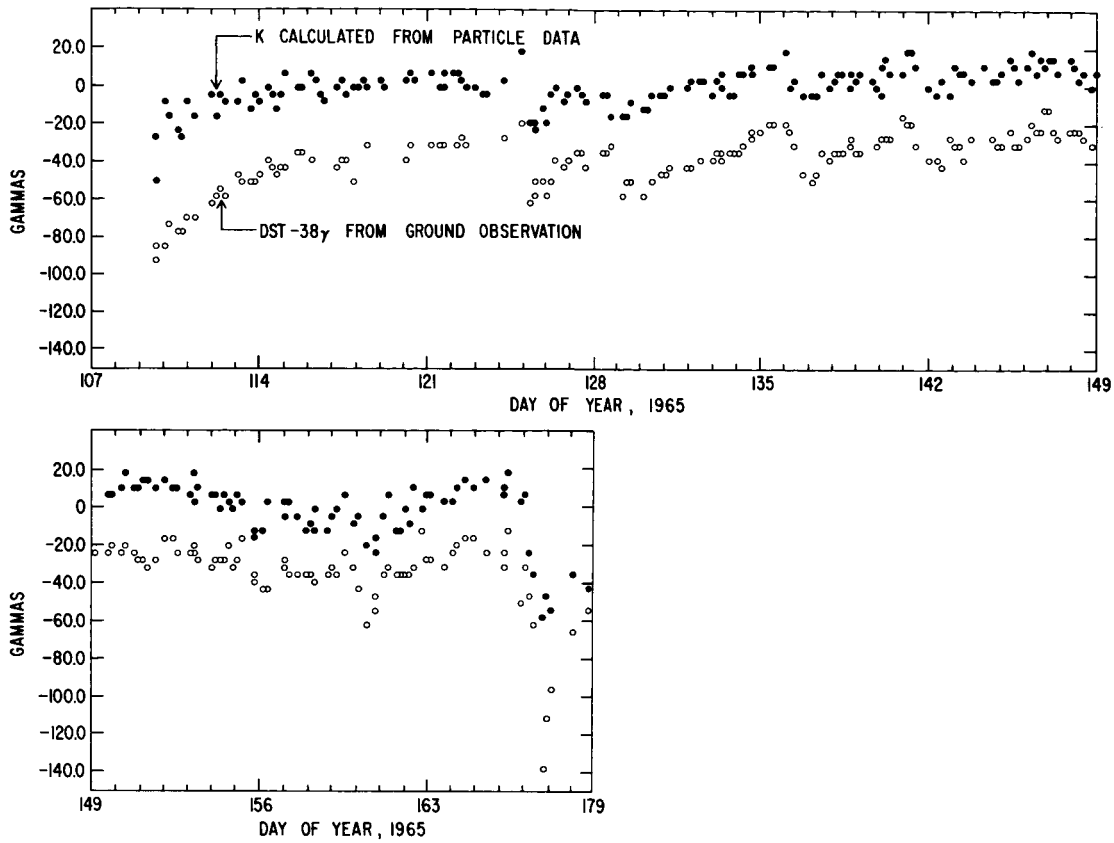

Figure 26. Dst values derived from ground observation and K derived from the particle data measured by Explorer 26, plotted as a function of time.

Table 5

The Linear Correlation Between K and Dst Expressed by $K = A \cdot Dst + B$. The Values of B and RMS are in Gammas.

Day of Year 1965	$A \pm \Delta A$	$B \pm \Delta B$	RMS	Correlation Coefficient
107-128	0.55 ± 0.05	-1.75 ± 0.80	6	0.81
128-149	0.66 ± 0.06	-0.16 ± 0.6	5	0.77
149-170	0.70 ± 0.05	-4.87 ± 0.9	8	0.86

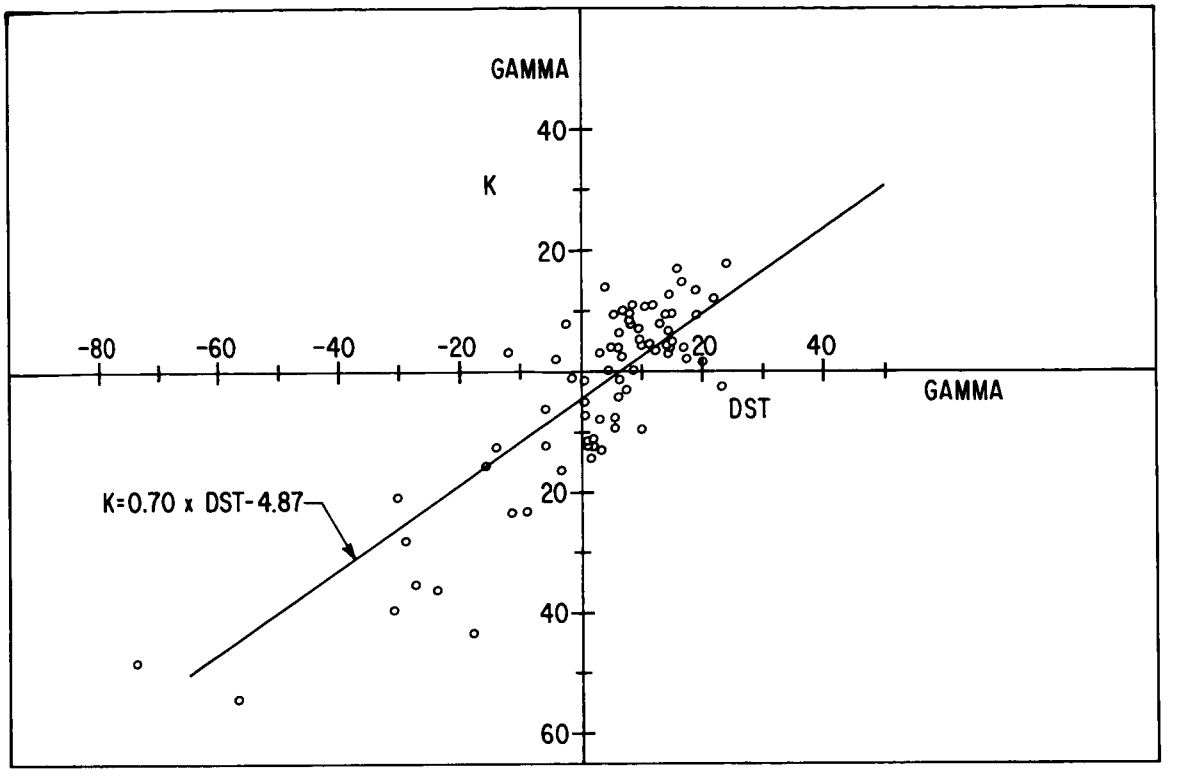

Figure 27. Scatter diagram showing the linear correlation between K and Dst for the days 149 to 170 of 1965.

the ratio between external and internal sources to the field is completely independent of any assumptions about the electrical conditions in the earth's interior and is solely based on the adiabatic behavior of the trapped particles. The values of A obtained in this way vary between 0.55 and 0.70 and are in fair agreement with the values calculated, taking into account the electrical conditions of the earth, and given in Table 4.

DISCUSSION AND CONCLUSIONS

The data presented here clearly demonstrates that build up and decay of the ringcurrent magnetic field as expressed by Dst cause a predictable adiabatic deceleration and acceleration of trapped protons inside the region L = 5. The

Dst values can therefore be used to remove the effects of these adiabatic changes and thus make it possible to study the non-adiabatic effects of the other processes with greater accuracy.

Preliminary results reported by Davis and Söraas (1968) show that the non-adiabatic changes in the April 18, 1965, storm occurred well into the main phase during a large polar substorm. Prior to the substorm the protons show only adiabatic changes as the main phase builds up. The non-adiabatic effects occurring during magnetic storms and have also been discussed by McIlwain (1966b) and Brown et al. (1967). Brown et al. show that the polar substorms play a key role in the physics of magnetic storms and of particle acceleration. They suggest that the polar substorm and particle accelerations (and losses) are due to an instability in the magnetosphere. The results of our study shows that the low energy protons are enhanced and the higher energies are greatly depleted after a geomagnetic storm.

This observation seems to explain the change in the proton intensities occurring between December 1962 and February 1965, reported by Davis and Williamson (1966). They find that the low energy protons in December 1962 is enhanced with respect to the same energies in February 1965 but for the high energy protons it is reversed, they are depleted in December 1962 with respect to the same energies in February 1965. Remembering that the last few months of 1962 was highly disturbed containing several geomagnetic storms Lincoln (1963) and that the time prior to February 1965 was quiet Lincoln (1965) and Lincoln (1966). Their observations are in agreement with our general result. This rapid change in the proton fluxes seems to penetrate deeper into the magnetosphere as the size of the storm increases. A model involving large scale electric fields in the magnetosphere during magnetic storms as suggested by Alfvén (1939, 1940, 1955, 1958), Block (1966) and others can qualitatively explain this. We are assuming a soft spectrum of the protons in the tail region and that these protons are drifted toward the earth by an electric field. As they move to regions of higher B value they are energized, resulting in a net increase in the intensity of low energy protons. At the same time higher energy protons which were trapped at a particular radial distance can become untrapped and be drifted by the electric field toward the front of the magnetosphere causing these energies to be depleted at a particular radial distance. The lower energy protons will drift closer to the earth than the depletion of the higher energy ones in agreement with the observations at $L = 3$, where the low energy protons are enhanced but where there are no depletions of the higher energies. The larger the storm, and presumably the electric field, the deeper the effects penetrate. Following the storm-time changes both the lower- and higher-energy protons slowly recover toward their prestorm values. The recovery rates increase with increasing L-value. It is clear that these storm-time connected processes play an important

role in controlling the population of the outer zone protons. They are different from L-diffusion proposed by Nakada and Mead (1965b) as a source of populating the outer zone protons. It seems reasonable to believe that both processes can operate but at different time-scales.

The processes invoking the plasma instability or E× B drift from the tail could account for the abrupt change in the fluxes in connection with magnetic storms. L-diffusion could play an important role for the time behavior of the fluxes after non-adiabatic processes operating on a short time scale have taken place. Fälthammer (1966) has shown that the power spectrum of the time variations of electric and magnetic fields enter into the diffusion coefficient of trapped particles. This means that a wide class of time variations in these field quantities will have an effect on the transport of charge particles in the magnetosphere and we need not only rely on the larger disturbances in order to transport particles across field lines.

Preliminary results reported by Söraas (1968) show that the behavior of the proton fluxes after the April 18 event are in qualitative agreement with the solution of a time dependent Fokker-Planck equation with transport and loss terms.

REFERENCES

Alfvén, H., A theory of magnetic storms and aurorae I, Kungl. Sv. Vetenskapsakad. Handl., Sec. 3, 18, no. 3, 1939.

Alfvén, H., A theory of magnetic storms and aurorae II, III, Kungl. Sv. Vetenskapsakad. Handl., Sec. 3, 18, no. 9, 1940.

Alfvén, H., On the electric field theory of magnetic storms and aurorae, Tellus, 7, 50, 1955.

Alfvén, H., On the theory of magnetic storms and aurorae, Tellus, 10, 104, 1958.

Armstrong, T.P., and S. M. Krimigis, "Observations of Protons in the Magnetosphere and Magnetotail with Explorer 33," J. Geophys.Res., 73, 143, 1968.

Block, L., On the distribution of the electric fields in the magnetosphere, J. Geophys. Res., 71, 855, 1966.

Brown, W. L., L. F. Cahill, L. R. Davis, C. E. McIlwain, and C. S. Roberts, "Acceleration of Trapped Particles During a Magnetic Storm on April 18, 1965," J. Geophys. Res., 73, 153, 1968.

Burns, A. L., "Effects of the 17 April 1965 Magnetic Storm on Trapped Protons," Dept. of Physics and Astronomy, Master Thesis, University of Iowa, February 1968.

Cahill, L. J. Jr., "Inflation of the Inner Magnetosphere During a Magnetic Storm," J. Geophys. Res., 71, 4505, 1966.

Chapman, S., and A. T. Price, "The Electrical and Magnetic State of Interior of the Earth, as Inferred from Terrestrial Magnetic Variations," Phil. Trans. Roy. Soc. London, A, 229, 427, 1930.

Davis, L. R., and F. M. Williamson, "Low-Energy Trapped Protons," Space Res. 3, 365, 1963.

Davis, L. R., R. A. Hoffman, and J. M. Williamson, "Observations of Protons Trapped above 2 Earth Radii," (Abstract) Trans. Am. Geophys. Union 45, 84, 1964.

Davis, L. R., "Low Energy Trapped Protons and Electrons," Proceedings of the Plasma Space Science Symposium, (Held at Catholic Univ. Washington, D. C., June 1963) D. Reidel Pub. Co. Dordrecht, p. 212, 1965.

Davis, L.R., and J. M. Williamson, "Outer Zone Protons," in Proc. NATO Adv. Study Inst., Bergen, Norway, August, 1965, Radiation Trapped in the Earth's Magnetic Field, Ed. by B. M. McCormac, D. Reidel Publishing Co., Dordrecht, Holland, 215, 1966.

Davis, L. R., and F. Söraas, "Nonadiabatic Changes in the 100- to 1700-keV Trapped Protons Observed During and Following Magnetic Storms," (Abstract) Trans. Am. Geophys. Union, 49, 231, 1968.

Davis, T.N., and M. Sugiura, "Auroral electrojet activity index AE and its universal time variations," J. Geophys. Res., 71, 785, 1966.

Dessler, A. J., and R. Karplus, "Some Effects of Diamagnetic Ring Currents on Van Allen Radiation," J. Geophys. Res., 66, 2289, 1961.

Eckhardt, D. H., "Geomagnetic Induction in a Concentrically Stratified Earth," J. Geophys. Res., 68, 6273, 1963.

Fälthammer, C. G., "On Transport of Trapped Particles in the Outer Magnetosphere," J. Geophys. Res., 71, 1487, 1966.

Hoffman, R.A., and P. A. Bracken, "Higher-Order Ring Currents and Particle Energy Storage in the Magnetosphere," J. Geophys. Res., 72, 6039, 1967.

Jensen, D. C., and J. C. Cain, "An Interim Geomagnetic Field," (Abstract) J. Geophys. Res., 67, 3568, 1962.

Kennel, C. F., and H. E. Petschek, "Limit on Stability Trapped Particle Fluxes," J. Geophys. Res., 71, 1, 1966.

Lincoln, J. V., "Geomagnetic and Solar Data," J. Geophys. Res., 68, 2335, 1963.

Lincoln, J. V., "Geomagnetic and Solar Data," J. Geophys. Res., 70, 2233, 1965.

Lincoln, J. V., "Geomagnetic and Solar Data," J. Geophys. Res., 71, 2411, 1966.

McDonald, K. L., "Penetration of the Geomagnetic Secular Variation Through a Mantel with Variable Conductivity," J. Geophys. Res., 62, 117, 1957.

McIlwain, C. E., "Ring Current Effects on Trapped Particles," J. Geophys. Res., 71, 3623, 1966a.

McIlwain, C. E., "Processes Acting Upon Outer Zone Electrons, I. Adiabatic Perturbations," Presented at Interunion Symposium on Solar-Terrestrial Physics, Belgrade, Yugoslavia, September 1, 1966b.

Mihalov, J. D., and R. S. White, "Low-energy Proton Radiation Belts," J. Geophys. Res., 71, 2207, 1966.

Nakada, M. P., J. W. Dungey, and W. N. Hess, "On the origin of outer-belt protons, 1," J. Geophys. Res., 70, 3529, 1965a.

Nakada, M. P., and G. D. Mead, "Diffusion of Protons in the Outer Radiation Belt," J. Geophys. Res., 70, 4777, 1965b.

Söraas, F., "Comparison of Post-Storm Nonadiabatic Recovery of Trapped Protons with Radial Diffusion," (Abstract) Trans. Am. Geophys. Union, 49, 232, 1968.

Takeuchi, H., and M. Saito, "Electromagnetic Induction Within the Earth," J. Geophys. Res., 68, 6287, 1963.